DISSERTATIONS IN
FORESTRY AND
NATURAL SCIENCES

Mihail Petrov

Glass-metal nanocomposites for photonics applications

Publications of the University of Eastern Finland
Dissertations in Forestry and Natural Sciences No 101

UNIVERSITY OF
EASTERN FINLAND

MIHAIL PETROV

Glass-metal nanocomposites for photonics applications

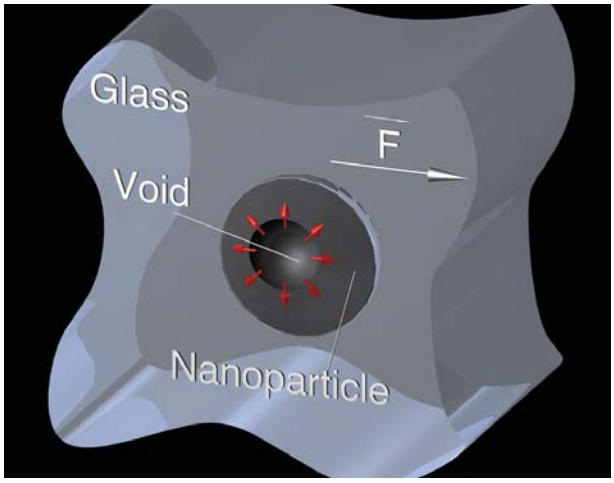

Publications of the University of Eastern Finland
Dissertations in Forestry and Natural Sciences
No 101

Academic Dissertation
To be presented by permission of the Faculty of Science and Forestry for public examination in the Auditorium M102 in Metria Building at the University of Eastern Finland, Joensuu, on April, 12, 2013,
at 12 o'clock noon.

Department of Physics and Mathematics

Kopijyvä Oy
Joensuu, 2013
Editor: Prof. Pertti Pasanen
Prof. Kai Peiponen, Prof. Pekka Kilpeläinen, Prof. Matti Vornanen

Distribution:
University of Eastern Finland Library / Sales of publications
P.O. Box 107, FI-80101 Joensuu, Finland
tel. +358-50-3058396 julkaisumyynti@uef.fi
http://www.uef.fi/kirjasto

ISBN: 978-952-61-1072-1 (printed)
ISSNL: 1798-5668
ISSN: 1798-5668
ISBN: 978-952-61-1073-8 (pdf)
ISSNL: 1798-5668
ISSN: 1798-5676

Author's address:
University of Eastern Finland
Department of Science and Forestry
P.O.Box 111
FI-80101 JOENSUU
FINLAND
email: mikhail.petrov@uef.fi

Supervisors:
Professor Yuri Svirko, Ph.D.
University of Eastern Finland
Department of Science and Forestry Sciences
P.O.Box 111
FI-80101 JOENSUU
FINLAND
email: yuri.svirko@uef.fi

Professor Andrey Lipovskii, Ph.D.
Saint-Petersburg Academic University RAS
Department of Condensed Matter
Khlopina 8/3
194021, SAINT-PETERSBURG
RUSSIA
email: lipovskii@spbau.ru

Reviewers:
Professor Walter Margulis, Ph.D.
Acreo Swedish ICT
Fiber optics sensors and applications labaratory
Electrum 236
16440, STOCKHOLM
SWEDEN
email: walter.margulis@acreo.se

Professor Stefano Pelli, Ph.D.
Institute of Applied Physics Nello Carrara
Department of Optoelectronics and Photonics
Via Madonna del Piano 10
50019 SESTO FIORENTINO
ITALY
email: s.pelli@ifac.cnr.it

Opponent:
Private-docent Gerhard Seifert, Ph.D.
Martin-Luther-Universitat Halle-Wittenberg
Institut fur Physik
Hoher Weg 8
06120 HALLE
GERMANY
email: gerhard.seifert@physik.uni-halle.de

ABSTRACT

This work is dedicated to theoretical and experimental investigations of electric field induced effects in glasses and glass-metal nanocomposites (GMN), glasses embedded with metal nanoparticles. The advanced models of charge transport during silicate glass poling were developed and studied both analytically and numerically. The theoretical predictions are compared with existing experiments showing good correspondence. The modeling of charge transport in GMN has allowed us to arrive at quantitative theory of the electric field assisted dissolution (EFAD) of metal nanoparticles in glass matrix. The estimations of dissolution time of individual silver nanoparticle in a silicate glass have been done. The numerical analysis of the electric field induced transport of the charge carriers allowed us to develop the theory of the optical bleaching of GMN. The predictions of the developed theory well correspond to the results of the performed experiments and demonstrate in particular that dynamics of the dissolution process strongly depends on the chemical content of glass matrix. 1D and 2D optical GMN-based periodic structures were fabricated using EFAD technique. The performed near field optical microscopy measurements revealed that the EFAD resolution can be as small as 150 nm. Theoretical calculations show that depending on the spectral region GMN-based structures can be employed as either phase or amplitude diffraction gratings. Finally, the results obtained in the Thesis demonstrate that EFAD technique can be applied for fabrication of submicron and subwavelength optical structures based on GMN.

Universal Decimal Classification: 538.958, 538.93, 535.421, 544.774, 681.7.02
PACS Classification: 73.20.Mf, 78.66.Sq, 78.67.Bf, 81.05.Pj, 42.25.Fx,42.79.Dj, 73.63.Bd, 66.30.hh, 42.70.Ce,66.30.H-, 77.22.Ej, 79.70.+q
Keywords: surface plasmon resonances, nanoimprint, diffraction gratings, photonic structures, glass poling, drift-diffusion transport, ionic conductivity, Rayleigh-Taylor instability

Preface

This Thesis is a summary of the work that has been done during the last several years I spent in UEF. I have got enough courage to say that the bigger part of what I had learned still has been left beyond this manuscript. For all that and much more I obliged to my supervisors, Yuri Svirko and Andrey Lipovskii, whose joint effort allowed me to make this work done. I deeply appreciate them for their guidance and deep concern either in the research or in me personally. I want to thank them for their nerve to accept and follow my own work style.

During my studies I felt a big support from many people in the Department of Physics and Mathematics. Huge thanks to Hannele Karppinen and Katri Mustonen who are the persons always ready to give an answer to all the naive and silly questions I usually have. I am very thankful to people from NanoCarbon group. Guys, all of you are very special and it was a pleasure to meet you and have a chance to work together. I want to give special thanks to Janne Laukkanen and Petri Stenberg who helped me to accommodate myself to cleanroom and fabricate proper experimental samples. Thanks to Jani Tervo for his help in the improvement of my theoretical background.

I feel gratitude to my parents and my family for their constant support. I want to note that they have made a big contribution to the obtained results, however none of them is included in the coauthors list.

Mihail Petrov

Joensuu, 13 February, 2013

LIST OF PUBLICATIONS

This thesis consists of the review of the author's work in the field of electric field induced processes in glasses and glass-metal nancomposites and the following selection of the author's publications:

I M.I. Petrov, A.V. Omelchenko and A.A. Lipovskii, "Electric field and spatial charge formation in glasses and glassy nanocomposite", *Journal of Applied Physics* , **109,** 094108 (2011). (With the permission of APS, lic. num. 3113680497167)

II M. I. Petrov, Ya. A. Lepenkin and A.A. Lipovskii, "Polarization of glass containing fast and slow ions", *Journal of Applied Physics*, **112**, 043101 (2012). (With the permission of APS, lic. num. 3113680503439)

III A. A. Lipovskii, V. G. Melehin, M. I. Petrov, Yu. P. Svirko and V. V. Zhurikhina, "Bleaching vs poling: comparison of electric field induced phenomena in glasses and glass-metal nanocomposites," *Journal of Applied Physics*, **109,** 011101 (2011). (With the permission of APS, lic. num. 3113680501027)

IV M. I. Petrov, V.G. Melehin and A.A. Lipovskii, "On the stability of elastic nanoparticles", *Physica Status Solidi B*, **249,** 2137–2139 (2012). (With the permission of Wiley Publishing, lic. num. 3113680505865)

V M. I. Petrov, V.G. Melehin, V. V. Zhourikhina, Yu. P. Svirko and A.A. Lipovskii, "Dissolution of metal nanoparticles in glass under DC electric field", *Journal of Physics D: Applied Physics*, **46,** 045302 (2013). (With the permission of IOP)

VI K.S. Sokolov, V.G. Melehin, M.I. Petrov, V. V. Zhurikhina and A.A. Lipovski, "On spatially periodical poling of silica glass", *Journal of Applied Physics*, **111,** 104307 (2012). (With the permission of APS, lic. num. 3113680499351)

Throughout the overview, these papers will be referred to by Roman numerals.

In addition the author has the following peer-reviewed journal articles

- A.I. Denisyuk, M. A. Tinskaya, M. I. Petrov, "Tunable Optical Antennas Based on Metallic Nanoshells with Nanoknobs", *Journal of Nanoscience and Nanotechnology*, **12**, 8246-8250 (2012).
- M. Dussauze, V. Rodriguez, A. Lipovskii, M. Petrov, C. Smith, K. Richardson, T. Cardinal, E. Fargin, E. I. Kamitsos, "How Does Thermal Poling Affect the Structure of Soda-Lime Glass?", *Journal of Physical Chemistry C*, **114**, 1275412759 (2010).
- P. Brunkov, V. Goncharov, V. Melehin, A. Lipovskii, M. Petrov, "Submicron surface relief formation using thermal poling of glasses", *e-Journal of Surface Science and Nanotechnology*, **7** , 617-620 (2009).

and international conference proceedings papers

- M.I. Petrov, Yu.P. Svirko, O.V. Shustova, A.A. Lipovskii, "Metamaterials based on glass metal nanocomposites", *Metamaterials 2012*, 17 -22 September 2012, St-Petersburg , Russia.
- M.I. Petrov, Yu.P. Svirko, O.V. Shustova, A.A. Lipovskii, " Glass-metal nanocomposites based diffractional gratings", *EOS Diffraction topical meeting*, 27 February-1 March 2012, Delft, Netherlands.
- M.I. Petrov, Yu.P. Svirko, O.V. Shustova, A.A. Lipovskii, "Glass-metal nanocomposites based diffractional gratings", *5th Finnish-Russian Photonics and Lasers Symposium*, 18-20 October 2011, St. Petersburg, Russia.
- A. I. Denisyuk, M. A. Tinskaya, M. I. Petrov, "Tunable Optical Antennas Based on Metallic Nanoshells with Nanoknobs", *Days on Diffraction*, 30 May - 3 June 2011, St. Petersburg.
- A. I. Denisyuk, M. A. Tinskaya, M. I. Petrov, "Tunable Optical Antennas Based on Metallic Nanoshells with Nanoknobs", *E-MRS ICAM IUMRS 2011*, 9-13 may 2011, Nice, France.

- A. A. Lipovskii, M. I. Petrov, V. G. Melehin, Yu. P. Svirko, "The Model of Electric Field Assisted Dissolution of Metal Nanoparticles in Glass", *Nanostructures: physics and technology*, 21-26 June 2010, St. Petersburg, Russia.

related to the research work.

AUTHOR'S CONTRIBUTION

The publications selected in this dissertation are original research papers on electric field induced effects in glasses and GMN as well as on the fabrication and characterization of GMN-based photonics structures.

The papers **I-VI** present results obtained by the team mentioned in the lists of authors. The main ideas were generated in fruitful discussions of all team members. In Paper **I**, the author has contributed to analytical and numerical solution of equations describing the carriers dynamics system and employed the obtained theoretical results to explain the experimental data. Bachelor student Ya. A. Lepenkin' led by the author has made significant contribution to the calculations presented in Paper **II**. In Paper **III**, the author has fabricated the surface relief gratings and performed estimations of nanoparticle dissolution dynamics. In Paper **IV**, the author has built the theoretical model and performed all analytical and numerical calculations. In Paper **V**, author of this Thesis has contributed to almost all stages of research: numerical calculations, fabrication and experimental work, comparison of experimental data and theoretical results. In Paper **VI**, the author has been involved in the building a numerical solution and in the discussion of obtained results.

Contents

1 Introduction

Artificial composite materials based on a properly arranged collection of nanoentities in an appropriate matrix have been recently emerged as an efficient alternative to conventional media in photonics applications. In particular these materials gave birth to photonics crystals allowing one to engineer bands for two- and three-dimensional subwavelength structures (2D and 3D, respectively) [1, 2], while ensembles of quantum dots in dielectric matrix were used as efficient saturable absorbers for mode-locking of solid-state lasers [3,4]. One may also recall split ring resonators that have been proposed as a model system with a negative refractive index [5] and opened the metamaterial race. Having very few counterparts in nature [6] artificial nanostructures are promising for development a wide variety of optoelectronics and photonics devices with enhanced and unusual functionality, ranging from superlenses to electromagnetic cloaks [7]. New functionalities can arise from resonances associated with either periodic spatial arrangement of nanoentities in the 2D or 3D array (e.g. in photonic crystals) or their intrinsic degrees of freedom (e.g. in quantum dot mode-lockers). However the most drastic enrichment in terms of functionality can be achieved when resonances of different nature can simultaneously contribute to the optical response. One may recall in this respect lasing when new functionality has been created by employing resonant coupling of the cavity eigenmodes to resonant quantum states of ions, atoms or molecules.

Glass-metal nanocomposites (GMN) are well suited for fabrication of photonic structures and metamaterials with tunable optical properties. GMN are glasses embedded with silver, copper, gold, nickel or other metal nanoparticles. GMN optical properties are governed by surface plasmon resonance (SPR) associated with collective oscillations of electrons in the metal nanoparticles. Field enhancement in the vicinity of a metal nanoparticles at the SPR

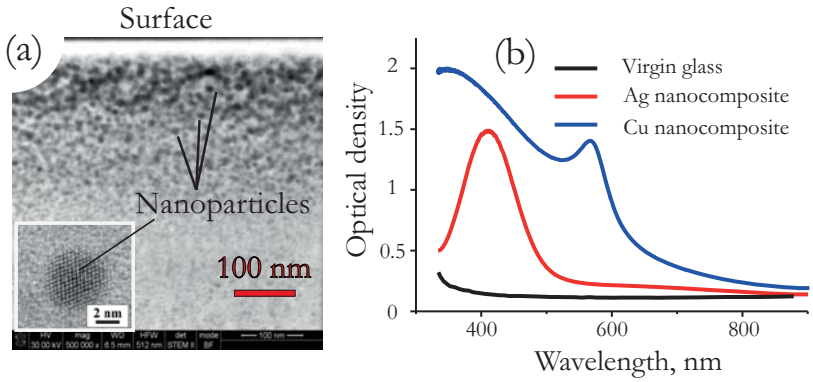

Figure 1.1: (a) TEM image of GMN crossection. Individual nanoparticles are clearly seen. Inset: High Resolution Electron Microscopy (HRTEM) image of 2 nm silver nanoparticle in glass (with permission from [8]) (b) Optical density spectra of virgin glass, silver, and copper glass-metal nanocomposites.

frequency results in strong optical nonlinearity of GMN leading to a variety of optical effects. In particular drastic enhancement of the third-order susceptibility of GMN in picosecond timescale is very prospective for optoelectronics applications [9]. Enhancement of the photoluminescence [10, 11] and SERS [12, 13] signals in the vicinity of individual nanoparticles make GMN attractive for development of novel active media for solid state lasers and biophotonics, respectively. It has been recently shown that GMN may be prospective for data storage application [14].

One of the most attractive features of GMNs is an opportunity to engineer their optical and electronic properties by nanopatterning. Specifically, the GMN can be bleached by applyingof DC voltage to the sample at elevated temperature [15–17]. It has been shown [15] that the bleaching is due to the electric field assisted dissolution (EFAD) of nanoparticles caused by drastic enhancement of electric field strength in the subsurface layer. The EFAD process opens a route for imprinting of 1D and 2D structures [18] using properly structured anodic electrode (stamp). Figures 1.2 (a) and 1.2 (b) show SEM image of the positive electrode (anode) used for imprinting

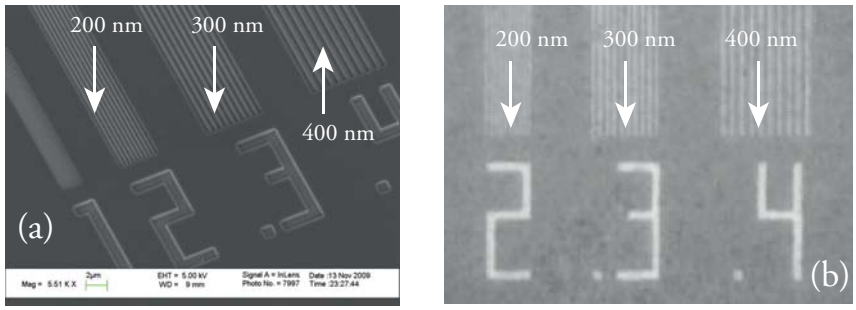

Figure 1.2: (a) SEM image of anode electrode. Numbers 1, 2, 3 and 4 correspond to line width of 100, 200, 300 and 400 nm. (b) Gratings imprinted in GMN via EFAD technique.

and an optical microscope image of gratings imprinted in the GMN. It is clearly seen from Fig. 1.2 b) that the grating of period of 300 nm is well reproduced. The lines with 200 nm width cannot be resolved by optical microscope.

EFAD technique allows fabrication of 2D [18, 19] and even 3D [20] periodic structures with submicron and subwavelength resolution. Taking into account nonlinear properties of GMN such structures may be used in actively developing field of nonlinear photonic crystals and metamaterials. Moreover, since this technique can be employed for imprinting of arbitrary structures in the GMN, one can use it for fabrication of optical planar circuits. That is the GMN may form a base for a cheap industrial technology of planar optical components fabrication. Detailed description of EFAD and imprinting techniques can be found in the chapters 3 and 4.

At elevated temperature, the DC electric field results also in the formation of surface profile that complements that of anodic electrode [21, 22]. The average height of the profile imprinted on the GMN surface is around tens of nanometers depending on fabrication conditions. Figure 1.3 (a) shows an example of the imprinted surface relief on GMN. The profile of anodic electrode used for imprinting is shown in the inset. The width of the imprinted structure line is 50 μm. However submicron relief formation is also possible and corresponding structures are shown in fig. 1.3 (b). Such a

technique can be applied for surface nanostructuring, in particular for fabrication of antireflection coatings, one of the most important problems in photovoltaics [23,24].

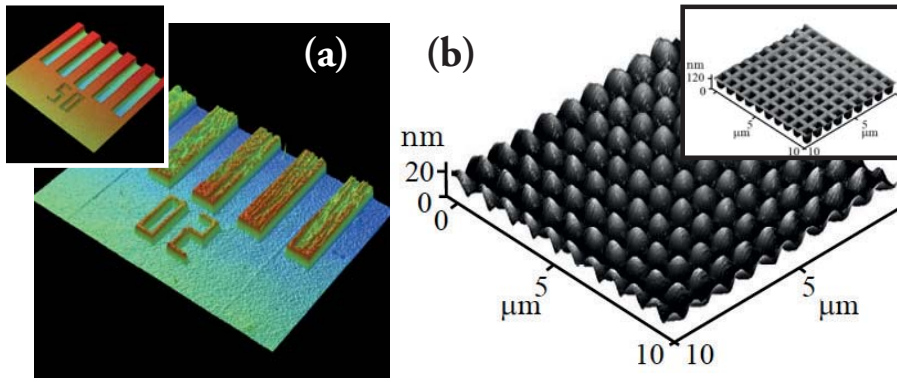

Figure 1.3: (a) Surface relief of GMN sample after thermal imprinting. Line width of formed lamellars equals to 50 μm. Inset: surface profile of electrode; (b) Atomic force microscopy of submicron relief profile on GMN surface after imprinting with electrode shown in the inset.

The GMN properties described above make GMN very prospective for linear and nonlinear optics and photonics, optoelectronics, biosensing, and photovoltaics. The Thesis is dedicated to investigation of GMN properties, development of GMN nanostructuring methods, fabrication and modeling of diffraction gratings based on GMN.

2 Glass–metal nanocomposites: optical properties, fabrication, characterization

2.1 LIGHT SCATTERING BY SPHERICAL PARTICLES. SURFACE PLASMON RESONANCE

The optical properties of GMN are governed by the resonant light scattering by metal nanoparticles embedded into glass matrix. The problem of light scattering by a spherical particle has been studied for more than 150 years. It has been first formulated by Clebsch [25] who studied scattering of elastic waves by a spherical inclusion. Despite the fact that Clebsch had not arrived at full solution of the problem, he was the first who considered variables separation in spherical coordinates. His research has made an important contribution in the development of the special functions theory. Clebsch had considered Rayleigh scattering ten years earlier than Lord Rayleigh in his work [26]. Large contribution to the scattering theory was made by Lamb, Lorenz, Thomson and others [27] in the late 19 annd early 20 century. Today the theory of light scattering by arbitrary spherical particle is referred as Mie theory after Gustav Mie, whose paper [28] was not the first on this subject but probably the most comprehensive by that time. In particular, Mie has considered spherical inclusion with complex permittivity. Together with Debyes work published in 1909 [29] Mie's paper has made a basis for the solution of light scattering problem that often referred to as Lorenz-Mie-Debye theory [30]. The modern representation of it can be found in Bohren and Huffman book [31].

Theory of light scattering had been advanced in 1940-1950's due to strong demand from industry and defense (development of var-

ious types of radars) as well as from physics of atmosphere and astrophysics [32]. However these researches were mainly focused on the far field. Recent advances in nanotechnology gave birth to photonics and plasmonics, which deal with properties of the electromagnetic waves at the wavelength and subwavelength scales. Control of local electric fields at the scales of tens and hundreds of nanometers opens a new route for optical devices for optoelectronics, biology and medicine.

In GMN, the local electric field can be strongly enhanced due to surface plasmon resonance (SPR) associated with collective oscillations of free electron gas in metal nanoparticles. Resonant scattering of light with metal nanostructures gives giant enhancement of local electric fields in the vicinity of nanoparticles. In this Thesis, we will consider only spherical metal nanoparticles embedded in glass matrix. Let us briefly review the basic concepts of the SPR in the quasistatic limit, i.e. when the light wavelength is much longer than the nanoparticle circumference, $\lambda \gg 2\pi R$, where R is nanoparticle radius. In this approximation, we can neglect variation of the electric field magnitude on the size of the particle. It is well known [33] that a sphere with permittivity ε_1 embedded in dielectric with pemittivity ε_2 and subjected to a uniform electric field accrues the dipole moment:

$$\boldsymbol{d} = \varepsilon_2 \alpha \boldsymbol{E},$$

where polarizability α can be expressed as

$$\alpha = \frac{\varepsilon_1 - \varepsilon_2}{\varepsilon_1 + 2\varepsilon_2} R^3.$$

The absorption and scattering cross-sections of the sphere with permittivity ε_2 are given by the expressions [31]:

$$\sigma_{abs} = 4\pi k_2 Im(\alpha), \qquad \sigma_{sca} = \frac{8\pi}{3} k_2^4 |\alpha|^2,$$

where $k_2 = \sqrt{\varepsilon_2} k_0$, where $k_0 = 2\pi/\lambda$ is the light wave vector in vacuum. One can observe that the absorption cross section is

proportional to k_0R, $\sigma_{abs} \sim k_0R$, while the scattering cross-section $\sigma_{sca} \sim (k_0R)^3$. Thus for small nanoparticles the absorption dominates over the scattering because $\sigma_{sca}/\sigma_{abs} \sim (\lambda/R)^2$. The SPR frequency ω_{SPR} can be found from the condition that the denominator in scattering or absorption cross section tends to zero:

$$|\varepsilon_1 + 2\varepsilon_2| \to 0.$$

Dielectric permittivity of noble metals (e.g. silver) can be expressed via Drude model [34]:

$$\varepsilon_1 = \varepsilon_\infty - \frac{\omega_p^2}{\omega(\omega + i\gamma)}, \tag{2.1}$$

where ε_∞ in high frequency dielectric permittivity, ω_p is plasma frequency of metal, and γ is damping factor that is proportional to reciprocal scattering time of electrons in metal. Neglecting damping one can readily obtain the SPR resonance frequency:

$$\omega_{SPR} = \frac{\omega_p}{\sqrt{\varepsilon_\infty + 2\varepsilon_2}}. \tag{2.2}$$

For silver and copper nanoparticles embedded into the soda-lime glass this expression gives SPR wavelength of about 420 and 560 nm, respectively. The SPR resonance is clearly seen in the optical density spectra of silver and copper GMN shown in Fig.1.1 (b). It is worth noting that in copper-based GMN, the sharp increase of the optical density in the blue part of spectrum corresponds to $3d \to 4s$ interband electron transitions responsible for reddish color of copper.

Equation (2.2) derived the frequency of the dipole resonance of electronic gas that dominates in scattering and absorption in small metal particles. However when nanoparticle size increases the higher multipole order resonances [35] (quadrupole, octapole etc.) become important. In the quasistatic approximation resonant frequency of n-th order multipole resonance can be found from the following condition [30,31]:

$$\varepsilon_1 + \frac{n+1}{n}\varepsilon_2 = 0.$$

In the framework of Drude model the frequency of the n-th order resonance equals to:

$$\omega_{SPR}^{(n)} = \frac{\omega_p}{\sqrt{\varepsilon_\infty + \frac{n+1}{n}\varepsilon_2}}.$$

It is worth noting that at $n \to \infty$, i.e. when there are many nodes of electric field over nanoparticle circumference, SPR resonance frequency tends to the frequency of surface plasmon-polariton propagating at the planar metal/dielectric interface [36]:

$$\omega_{SPR}^{(n)} \xrightarrow[n\to\infty]{} \omega_{SPP} = \frac{\omega_p}{\sqrt{\varepsilon_\infty + \varepsilon_2}}.$$

That is the more periods of the light wave can be placed on the the particle circumference, the closer spherical surface of the nanoparticle is to the flat plane.

2.2 SILICATE GLASSES

2.2.1 Glass structure

In this Thesis, we consider only *silicate* ("soda-lime") glasses based on SiO_2 network. Fig. 2.1 a) shows a structure of silica glass based on amorphous random network. In the silica glass, the basic element is a tetrahedra with silicon atom in the center and four oxygen atoms in the vertices forms (in the projection shown in Fig. 2.1 only three bonds for each Si atom are seen). Each pair of silicon atoms is connected via an oxygen atom that is called "bridging oxygen". Impurities concentration in silica glass usually does not exceed 10-1000 ppm.

Soda-lime glass has SiO_2 amorphous network either, but in the contrary to silica glass, the concentration of additional components (modifiers) may be as high as 25 wt % (see Table 2.1). The main modifier in soda-lime glass is sodium oxide. Absolute concentration of Na atoms in the soda-lime glass is about $5 \cdot 10^{21}$ cm^{-3}. Sodium atoms are bonded with so called "non-bridging" oxygen

ions as it is shown in Fig. 2.1 (b) and have partial charge +1. Ca atoms are bonded to two non-bridging oxygen atoms and have partial charge +2.

Table 2.1: Typical content of soda-lime glass

Oxide	Na_2O	Al_2O_3	MgO	CaO	SiO_2
Wt. %	15,4	1,1	2,8	8,0	73,6

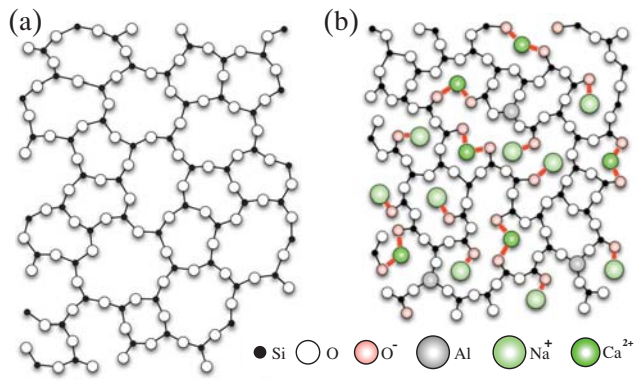

Figure 2.1: Amorphous structure of silica glass (a) and soda-lime glass (b)

2.2.2 Charge transport

At elevated temperatures silicate glasses exhibit ionic conductivity due to relatively low (below 1 eV) activation energy of alkali ions. In the case of soda-lime glasses the temperature of 200-300^0 is sufficient to stimulate migration of sodium ions under electric field. This can be considered as switching of sodium chemical bonds from one non-bridging oxygen atom to another. Calcium ions also participate in the transport but they have two bonds with glass network that makes their mobility much lower than sodiums. Thus at elevated temperature silicate glass can be considered as solid electrolyte with

Arrhenius type mobile spices. Diffusion coefficient can be written as:

$$D = D_0 \exp\left(-\frac{Q_a}{kT}\right),$$

where D is the self-diffusion coefficient, Q_a is the activation energy, kT is the thermal energy. Mobility and self-diffusion coefficient are connected via Nernst-Einstein relation:

$$\frac{\mu}{D} = \frac{e}{HkT},$$

where e is electron charge, and Haven constant $H \sim 0.3$ for soda-lime glasses [37].

Analisys of experimental data presented in the literature gives an estimation of sodium activation energy in soda-lime glass $Q_a \approx 0,8$ eV.

2.3 FABRICATION OF GMN

Two main techniques of GMN fabrication are ion implantation [38] and ion exchange [39,40].

Ion implantation technique is based on the bombardment of the glass substrate with metal ions with energy of 30 to 200 keV. Accelerated ions penetrate under the substrate surface and form a layer saturated with metal ions at the depth of hundred nanometers. Consequent annealing of the sample leads to neutralization of implanted ions and activation of the nanoparticles growth. Both distribution of ions after implantation and diffusion processes during nanoparticle growth define the spatial distribution of formed nanoparticles.

Although the ion implantation technique enables formation of high concentration of nanoparticles in the subsurface layer of glass, it is not a cost-effective. GMN fabrication based on the self assembled growth of nanoparticles using ion exchange process is much more common. It includes of two stages:

- Ion exchange. Soda-lime glass substrate is placed in a melt of the mixture of sodium nitrate and silver nitrate ($NaNO_3 -$

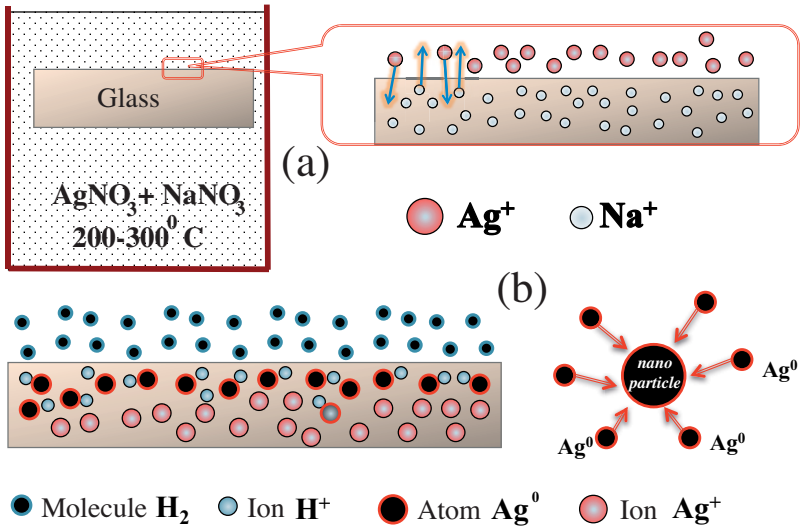

Figure 2.2: (a) Ion exchange process; (b) hydrogen reduction.

$AgNO_3$) at temperature of 320-350^0 C. High temperature activates diffusional migration of Na^+ ions out the glass surface and migration of Ag^+ ions inside glass via available non-bridging oxygen sites (see Fig. 2.2). Thus, after the ion exchange processing the subsurface region of the glass is enriched with silver ions chemically bonded with glass network: Ag-O–Si$\equiv O_3 \equiv$ ....

- Hydrogen reduction. After the ion exchange the glass substrate is placed into hydrogen atmosphere at temperature of about 300^0 C. Hydrogen molecules penetrate into the glass, and hydrogen atoms replace silver ions bonded with oxygen:

$$2\left(Ag^+ - O^- - ...\right) + H_2 \rightarrow 2(H^+ - O^- ...) + 2Ag^0$$

Reduced silver atoms start to precipitate forming silver nanoparticles, which size and spatial distribution in the glass matrix can be tuned by changing temperature and other parameters of the process.

2.4 CHARACTERIZATION OF GMN SAMPLES

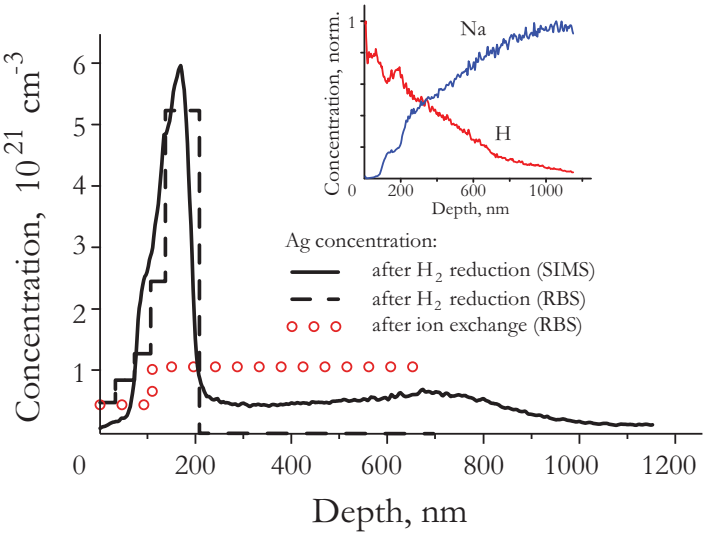

Figure 2.3: Silver concentration profile in the glass matrix after ion exchange and hydrogen reduction obtained using RBS and SIMS techniques. Inset: Concentration profile of Na and H ions after hydrogen reduction (normalized by maxima).

Fabricated nanocomposites have been characterized using Secondary Ion Mass Spectrometry (SIMS) and Rutherford Back Scattering (RBS) techniques. The obtained results show that silver nanoparticles are located at the depth of several hundred nanometers under the glass surface. Figure 2.3 shows profiles of silver concentration in glass before and after hydrogen reduction measured using SIMS and RBS. One can see that after ion exchange the concentration of silver in ionic state is almost uniform at the scale of 600 nm while its penetration depth during diffusion is several microns. Low concentration of silver at the glass surface is due to the existence of 50-100 nm thick subsurface dealkalined layer in which almost all alkali ions are substituted with ions taken form the atmospheric water vapors. After hydrogen annealing silver atoms start to migrate from the glass depth to the surface where the concentration of penetrating hydrogen is high. Thus a nanoparticle concentration

is maximal at the depth of 150 nm beneath their surface. Both RBS and SIMS measurements revealed that the width of the nanoparticle distribution about 100 nm. Approximate value of filling factor at the depth where the silver concentration is maximal is $f \approx 0.08$.

Thus it is necessary to stress that major part of silver nanoparticles is located at the depth of about 200 nm under the glass surface and that nanoparticle concentration rapidly decreases deeper in the glass.

3 Charge transport in glasses and glass-metal nanocomposite under DC electric field

Early studies of EFAD revealed that charge transport in glasses play very important role in this process [15]. EFAD is also referred to as poling assisted bleaching because of its similarity to well-known phenomenon of glass poling [41–43], which is governed by the charge redistribution in glass when an external voltage is applied at elevated temperature. However the term ”poling” is usually associated with the DC field induced second-order non-linearity of glasses. In both EFAD and glass poling processes, DC voltage applied to the glassy slab at elevated temperature [17, 18, 44] creates a strong electric field in the subanodic layer [20, 45]. The drift of ions in field results in the depletion of the subsurface layer with metal ions, preferably sodium ones. Glass poling manifests itself as the decrease in glass conductivity [46] and the formation of spatial charge in the subsurface glass layer. Poled glasses have attracted a considerable attention because the internal electric field created by the spatial charge breaks the inversion symmetry and hence permits the Pockels electro-optic effect [47] and second harmonic generation [41] in the glass. Thus studying of glass poling is important for both revealing EFAD process origin and for poled glasses applications in optics and photonics.

Charge transport in glasses can be described by the system of diffusion-drift equations:

$$\frac{\partial C_i(\mathbf{r},\mathbf{t})}{\partial t} + \nabla \cdot \mathbf{j_i}(\mathbf{r},t) = 0 \tag{3.1}$$

$$\mathbf{j_i}(\mathbf{r},t) = \mu_i \mathbf{F}(\mathbf{r},t) C_i(\mathbf{r},t) - D_i \nabla C_i(\mathbf{r},t), \tag{3.2}$$

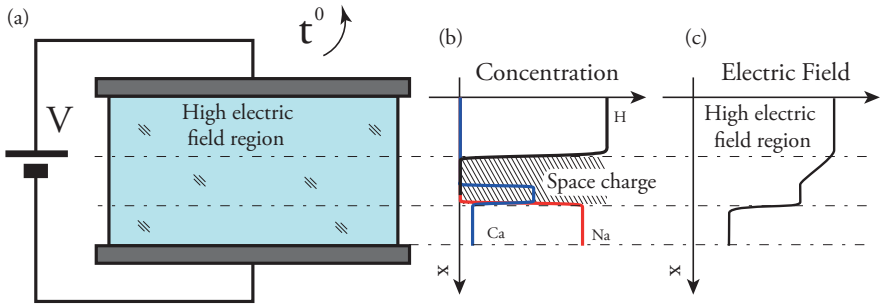

Figure 3.1: (a) The scheme of the glass poling process that takes place at elevated temperature and DC voltage. (b) Redistribution of the carriers during poling and consequent electric field build up (c).

where subscript labels type of carriers, C_i is charge carrier concentration, $\mathbf{j_i}$ is the total i-th carrier flux that contains both diffusional and drift components, $\mathbf{F}$ is the local electric field. In the course of the carrier redistribution local electric field is being built up and driving the carriers drift. Since the ionic transport is relatively slow, the Poisson equation may be used to describe carrier concentration and local electric field:

$$\nabla \cdot \mathbf{F}(\mathbf{r}, t) = \frac{e}{\varepsilon\varepsilon_0}\left(\sum_i q_i C_i - C_0\right), \tag{3.3}$$

where q_i is i-th carrier charge and C_0 concentration of nonbridging oxygen atoms (see Fig. 2.1). As it was mentioned in the previous chapter alkali and alkali-earth ions are responsible for the charge transport in silicate glasses. Positively charged ions switch their bonds from one nonbridging oxygen atom to another, while oxygen atoms do not participate in charge transport as they are tightly connected to silicon atoms. [1]

[1] It is worth noting that although the oxygen and electron transport had been discussed in [42, 48, 49], mechanisms behind the negative charge transport in silicate have not been properly explained yet. One may expect that in some cases the transport of negative and positive ions takes place simultaneously [50] being activated by high electric field. However in this Thesis, we do not consider the transport of the negatively charged carriers.

In the geometry shown in Fig. 3.1 the system of equations (3.2-3.3) can be reduced down to one-dimensional problem, i.e. the charge concentration C_i, flux density j_i, and electric field F being functions of depth x and time t.

The system of equations that govern field induced charge transport in glass yields:

$$\begin{gathered}\frac{\partial C_i(x,t)}{\partial t}+\frac{\partial j_i(x,t)}{\partial x}=0,\\ \frac{\partial F(x,t)}{\partial x}=\frac{e}{\varepsilon\varepsilon_0}\left(\sum_i q_i C_i - C_0\right),\\ j_i(x,t)=\mu_i F(r,t)C_i(r,t)-D_i\frac{\partial C_i(r,t)}{\partial x},\quad i=1..n,\end{gathered} \tag{3.4}$$

where j_i and F are x-components of the i-th carrier flux and electric field vectors. Boundary and initial conditions for drift-diffusion equations system (3.4) dependend on the specific problem. The electric field distribution in glass should satisfy the following relation:

$$\int_0^L F(x,t)dx = V_0,$$

where L is the sample thickness and V_0 is the applied voltage.

Silicate glass poling was considered in papers **I** and **II** devoted to the theory of charge transport on the basis of system 3.4 . When the diffusion component of the total current is neglected, 3.4 is reduced down to the system of the first order differential equations, which can be solved analytically. This nonlinear system has discontinuous solutions, which are referred to as shock wave solutions [51, 52]. This approach was developed in papers **I** and **II** to describe the poling of the two components sodium-silicate glass and poling of the glass additionally containing low-mobile Ca ions. To account the contribution of the diffusion to the ion redistribution current the system (3.4) was studied numerically. It was shown that diffusion smears the carrier profiles at the concentration frontiers and do not significantly affect the glass poling dynamics.

The process of poling of GMNs resembles that of virgin silicate glasses they are based on. However in GMN, the process dynamics

differs considerably because of different initial conductivity of glass and GMN. One of the main effects is that GMN poling results in nanoparticle destruction as it was mentioned above. Comprehensive comparison of glass and GMN thermal poling and the analysis of GMN poling was done in paper **III**.

4 Electric Field Assisted Dissolution of Nanoparticles

The electric field modfication of GMN was first reported in 2004 by Deparis et al. [15]. In order to enhance second-order nonlinearity they performed poling of the the glass containing silver nanoparticles. It has been discovered that poling resulted in destruction of silver nanoparticles and optical bleaching of the sample. Several years later electric filed assisted dissolution of gold [16] and copper [17] nanoparticles was also demonstrated.

Since the early studies [53] it has been suggested that nanoparticles dissolution has strong connections to thermal poling of glass. High electric field (up to 1 V/nm [45]) built up in the sub-anodic region owing to formation of spatial charge is responsible for nanoparticles dissolution. However, despite the advances in the GMN bleaching ***complex modeling of EFAD process has been accomplished only very recently in paper V***.

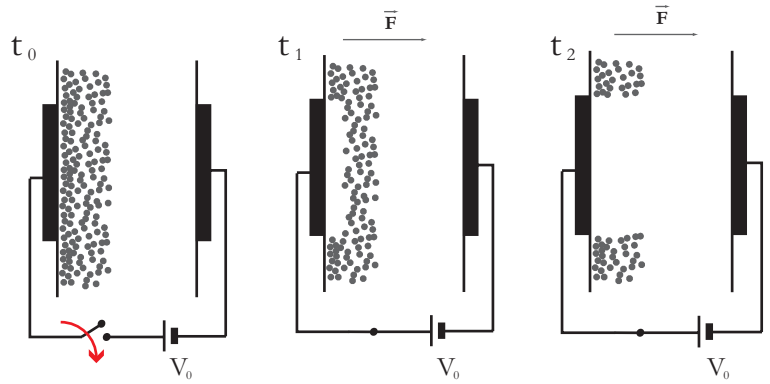

Figure 4.1: The scheme of EFAD process at time moments $t_0 < t_1 < t_2$. The process takes place at temperature of 200-300^{0}C. The dissolution of nanoparticles occurs only beneath the anode allowing fabrication of submicron structures shown in Fig. 1.2.

4.1 METAL NANOPARTICLES IN STATIC ELECTRIC FIELD

Conventional qualitative models of nanoparticle destruction in the presence of static electric filed [15,53] rely upon the *continuous* process of ion and electron emission into the glass matrix. However such a gradual decrease of the nanoparticle size is not the only possiblity. It is well known from early works of Lord Rayleigh [54] that charged liquid droplets tend to fragment if the Coulumb energy becomes higher than the surface tension energy. This condition implies that electric field induced stress dominates over the Laplace pressure under curved spherical surface. This instability, which is often referred as Coulumb or Rayleigh instability, can lead to explosion of liquid particles. Inhomogenuity of the electric field may also cause particle destruction when the electro-static energy of polarized sphere is higher than surface tension energy. This instability is also called Taylor instability after G. Taylor's pioneer works in 1964 [55]. These two instability mechanisms can be responsible for explosion-like destruction of charged liquid particles.

Thus problem of charged particle instability was discussed for liquid particles only. To the best of our knowledge there are no studies related to instability of solid metal nanoparticles embedded in solid matrix. Although melting temperature of nanoparticles is lower than that of bulk media, they remain solid in the EFAD process. For example, melting point of silver decreases from 1036^0 C for bulk down to 450^0C [56] for nanoparticles of 4 nm diameter, being still higher than the temperature range of EFAD process that is 200-300^0C. However, whilst metal nanoparticles stay solid, the EFAD process temperature is high enough to activate electric field induced ion migration in glass, which leads to the building up of high electric field in the subsurface region and charging the nanoparticles. The detailed analyses of metal nanoparticle stability during EFAD process was done in the paper **IV**. It has been shown in particular that the nanoparticles are stable at the electric field strength built up inside the glass matrix. Thus we can conclude that *instability does not affect the EFAD process provided that electric charge*

of the nanoparticle does not exceed the threshold value. This threshold charge was estimated in paper **IV**.

While electro-static instability is unlikely involved in the EFAD process, it may manifests itself the processing of metal nanocomposite with intense ultrashort light pulses [57, 58] that can result in explosive-like metal nanoparticle destruction [59, 60]. Depending on the conditions, two mechanisms of metal nanoparticle destruction by intense laser pulses can be distinguished: thermally or electric field activated evaporation [59, 60] and Coulomb explosion [61,62]. While the evaporation corresponds to heating of metal nanoparticle due to the transfer of energy from excited electronic system to the ion core, the mechanism of Coulomb explosion involves fast excitation of electronic system with consequent charging of the nanoparticle via electron or ion emission. Thus, nanoparticle can be charged before melting and according to studies presented in paper **IV** Coulumb instability of metal nanoparticle may lead to explosion-like destruction that was observed in the experiment [58].

4.2 DISSOLUTION OF NANOPARTICLES VIA ION EMISSION

The destruction of nanoparticles in electric field resembles well-known phenomena in solid-state physics. The first one is ion evaporation in high electric field that forms the basis of ion microscopy [63, 64]. Although the local electric field strength at the surface of metal nanoparticle in glass is almost one order lower than the electric field strength in the ion microscopy, it is high enough to activate ion emission into glass. This is because the emission barrier in glass matrix is lower than in vacuum. The second phenomenon is the electric field assisted dissolution of silver [65] and copper [66, 67] films deposited on the glass surface. This effect has been used for a long time for fabrication of optical waveguides in glass [65]. In these experiments, metal ions from the film were transferred into glass matrix under applied static electric filed and participate in charge transport together with intrinsic alkali carriers under external voltage of 100-200 V. This process can be seen as electrolyses of

metal electrode with glass playing a role of a solid electrolyte.

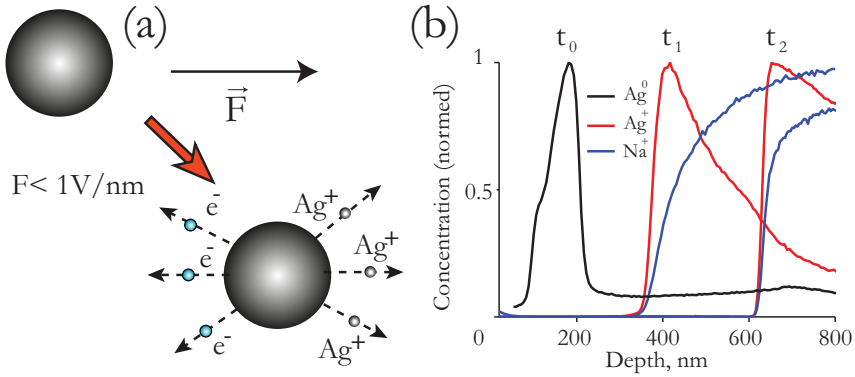

Figure 4.2: (a) Scheme of nanoparticle destruction via ion and electron emission in intensive electric field. (b) SIMS measurements of silver concentration in nanocomposite before (Ag^0) and after (Ag^+) EFAD with different treatment time. Sodium distribution is also shown. Applied voltage was 600 V at 230 ^{0} C.

The important difference between the electric field assisted dissolution of metal nanoparticles and metal films process is that the metal nanoparticles have no direct electric contact to anode. This indicates that in the EFAD is governed by the charge accumulation and that the key issue is the mechanism of electron emission from nanoparticles. In [53], electron tunneling from one metal particle to another has been proposed as the mechanism of negative charge emission. However this mechanism may be significant for nanocomposites with high nanoparticle concentration when average distance between nanoparticles is small. It unlikely can play the major role in the nanoparticle destruction in strongly diluted nanocomposites reported in [68]. Moreover, the dissolution of nanoparticle goes as a frontier from anode to cathode as it is shown in Fig.4.2. Thus the tunneling mechanism should be blocked as soon as no nanoparticles remain in the vicinity of the anode.

The mechanism of nanoparticle dissolution is not studied well especially at the last stages when the most metal atoms have been transfered from the nanoparticle to glass matrix. However, it has

been shown recently [69] that nanopores are formed in glass after nanoparticle dissolution. Small angle x-ray spectroscopy revealed that spatial and size distribution of pores coincides with that of nanoparticles. Indirect proof of pores formation was also shown in [70]. The pores have been also observed in [23] when static electric filed had been applied to glass sample with nanoparticles grown on its surface. SEM images of spherical nanoparticles at different stages of dissolution are shown in Fig.4.3. One can see that nanoparticle change their size and shape during dissolution, and nanopores are formed after the total destruction of nanoparticles.

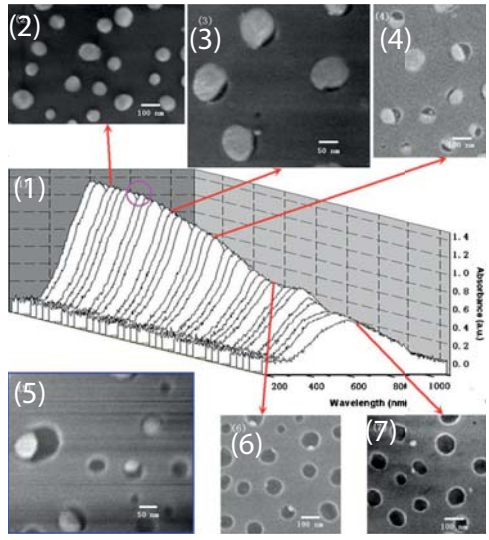

Figure 4.3: (1) Optical density spectrum of the glass sample with silver nanoparticles grown on its surface at different stages of dissolution. (2-7) SEM pictures of partially dissolved nanoparticle ***on the glass surface****. Picture has taken with permission of publisher from [23].*

By exploring existing concepts and experimental results author has developed the quantative model of the EFAD process that has no analogues in the literature. The model describes the electric field formation and charge transport in GMN in the course of poling process. The detailed description of it can be found in paper **V**.

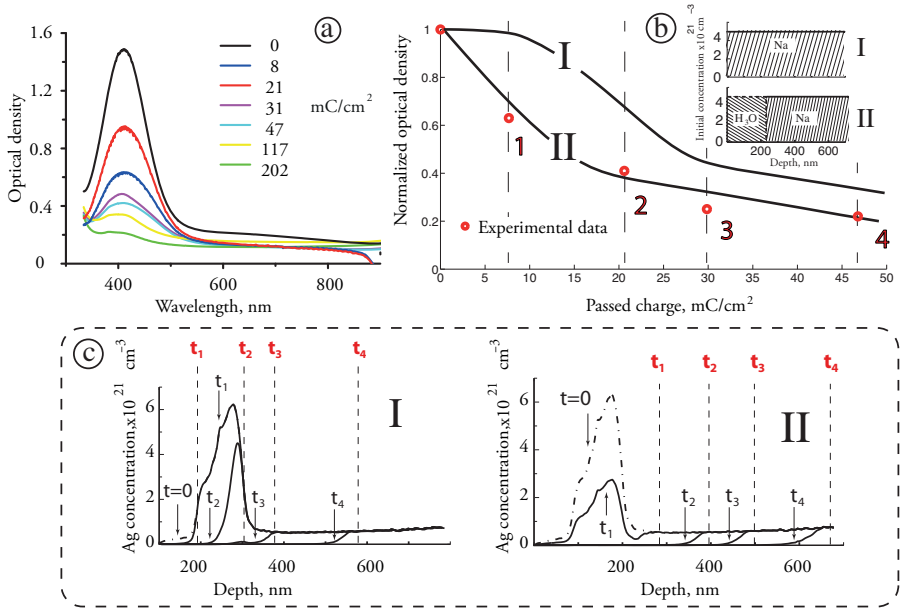

Figure 4.4: (a) (a) shows optical density spectra of GMN after EFAD at several passed charge densities. One can see the bleaching of the SPR due to nanoparticle dissolution; (b) Maximal optical density dependence on passed charge (circle scatter corresponds to experimental studies, line I and II corresponds to different initial concentration of sodium and hydrogen ions, shown in (b) inset); (c) Profile of silver concentration in nanoparticles for different initial concentration shown in Fig. (b) inset. Figure is adopted from **V**

The dissolution time of metal nanoparticle in glass matrix was obtained using estimated ion and electron emission energy barriers. The developed model well corresponds to the experimental data and allowed us to reveal most important parameters that influence EFAD dynamics. In Fig. 4.4 (a) the spectra of GMN samples after EFAD is shown for different passed charge density. One can see the decrease in optical density (optical bleaching) due to nanoparticle dissolution. In Fig. 4.4 (b), the dependence of optical density at the SPR on passed charge is shown with circle scatters. Solid lines show results obtained using the developed EFAD model.

Different initial ion distribution in GMN before the electric field is applied are considered. Line I represents results of the GMN

bleaching modeling assuming initially uniform distribution of sodium ions in glass matrix (see inset I Fig. 4.4). One can clearly see that in such a case results the experiment and modeling are quantitatively different. However, it has been shown [71,72] that after nanoparticle formation the subsurface are of glass is saturated with hydrogen that can form hydronium complexes bonding with non-bridging oxygen atoms. Line II represents the results of the modeling under assumption that hydrogen is homogeneously distributed in 200 nm thick layer (Fig. 4.4 (b)). The obtained results corresponds well to the experimental data showing that initial chemical content of GMN significantly influences the EFAD dynamics. In particular, high content of hydronium in GMN influences the redistribution of electric field inside the glass. In Fig. 4.4 (c) the modeled dynamics of nanoparticles dissolution is shown for different time moments corresponding to experimental point in Fig. 4.4 (b). In the absence of hydronium (see Figure 4.4 (c) I), the dissolution goes with frontier as hydronium starts to penetrate from the surface. When the hydronim content is high in the subsurface layer (see Fig. 4.4.(c) II), intense electric field is formed in the whole region containing nanoparticles immediately after applying external voltage and simultaneous dissolution of all the nanoparticles is observed.

5 Fabrication of optical structures

Development of telecommunication systems and rapid growth of informational technologies demands new methods of optical data processing and novel devices based on plasmonic chip-scale technology. These novel devices should exhibit both high data processing rate and have small critical dimensions due to high confinement of plasmonic waves [73]. Among plasmonic components that currently attract a widespread attention of the research community are waveguides, couplers, ring resonators [74–76]. One of the major problems here is high costs of plasmonic structures fabrication. The typical dimensions of plasmonic waveguides are well below the spatial resolution of photolithography process. Thus these structures should be fabricated using electron beam lithography (EBL), which enables typical dimensions of tens of nanometer. However implementation of the highly expensive and time consuming EBL-based fabrication of plasmonic components in wide scales is questionable. This makes important to search for alternative techniques of the subwavelength surface structuring. In [76] nanoimprint lithography is proposed for the fabrication of on-chip plasmonic circuits based on metal films. In particular, effective medium theories predict negative dielectric permittivity of GMN in the vicinity of the SPR and the propagation of surface plasmon polariton modes, which have recently been observed in [77–79]. It makes GMN attractive as a material for plasmonics and photonics components. It was already mentioned in the Introduction that one possible solution is nanostructuring of GMN using teh EFAD process [72].

Imprinting of plasmonic nanostructures in GMN is based on change of the nanoparticles density in the subsurface layer of glass via EFAD technique. The scheme of the EFAD-based imprinting

process, which has allowed us to imprint test structures with 600 and 800 nm linewidth is shown in the fig. 5.1 (a). The SEM image

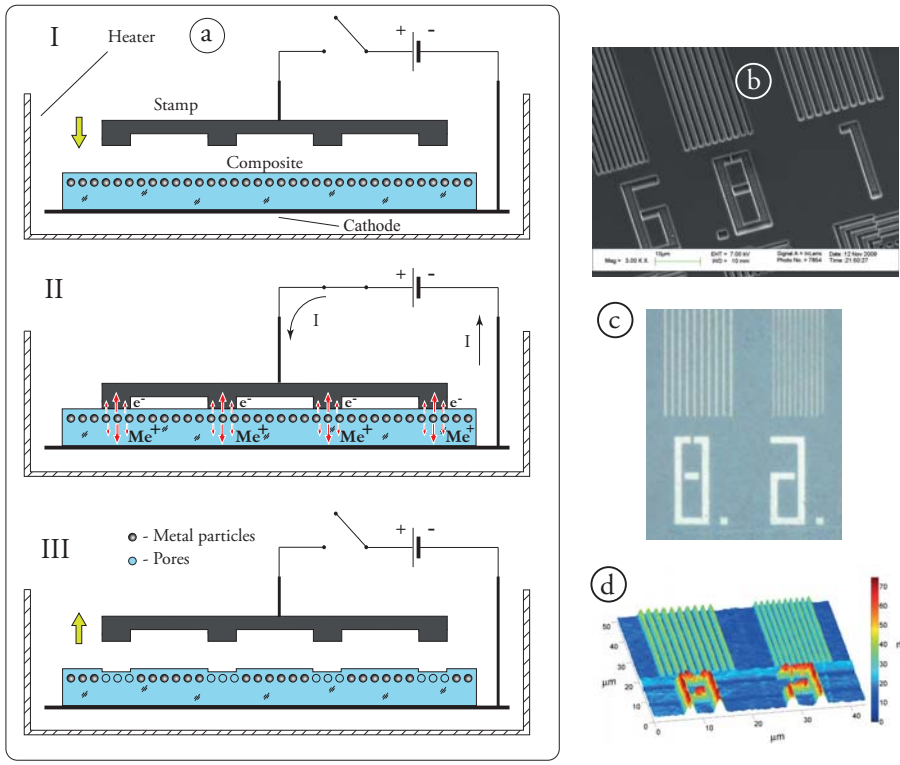

Figure 5.1: (a) The consequent stages of the EFAD imprinting process. (b) SEM image of anode surface. (c) Optical microscope image (reflection regime) of the GMN surface after EFAD imprinting. (d) AFM image of the GMN surface after imprinting.

of profiled anode is shown in fig. 5.1(b). The optical microscope image of the GMN surface in reflection mode is shown in Fig. 5.1 (c). One can see the clearly imprinted subwavelength structure. The brighter lines correspond to glass regions embedded with nanoparticles that gives rise in the reflectance. Along with the dissolution of nanoparticles formation of surface profile that complements stamp profile is observed [22,70]. The image surface profile with height of tens of nanometers obtained with optical profiler is shown in Fig. 5.1(d). Surface profiling occurs due to the volume defects, which

are formed in the glass matrix through the evacuation of alkali ions from subanodic region towards cathode. It is important to stress that the static electric field applied results in the formation of the surface profile of nearly the same height in glasses and GMN [69]. This clearly indicates that nanopores, which are created in the subanodic area in the GMN due to nanoparticles dissolution [70], have a minor effect on the profile formation.

Despite the results in imprinting of surface structures there are still remain fundamental problems that prevent fabrication of GMN based plasmonic and photonic components using EFAD. One of the important questions to be answered in this respect is spatial resolution of thermal imprinting process. It is already shown that nanoparticle concentration can be controlled in the submicron scale [18, 19]. In this Thesis, we demonstrate GMN structures with line width as low as 300 nm (see Fig. 1.2 (b)) imprinted using EFAD technique. To measure the resolution of imprinting beyond the diffraction limit of optical microscopy we employed the scanning near-field optical microscopy (SNOM).

5.1 RESOLUTION OF GMN IMPRINTING

To determine the resolution of the EFAD process, a profiled glassy carbon stamp was fabricated using EBL. The stamp represented a set of grooves varying in width from 100 to 500 nm with increment of 50 nm, and from 500 to 1100 nm with increment of 100 nm. The grooves depth was 350 nm, and the distance between the grooves was 2 μm. The stamp was used as an anode for the EFAD imprinting of GMN sample and virgin glass [80]. The imprinting was carried out at the temperature of 250^0 C and voltage 600 V applied to 1 mm thick sample.

The imprinted structure that is the set of GMN strips was tested using AFM and SNOM techniques. The results of the AFM measurements performed with AIST-NT SmartSPM scanning probe microscope are shown in Fig. 5.2. One can observe that the imprinted surface profile complements that of carbon stamp [22, 70]. It is

worth noting that the formation of the profile is not connected to the relaxation of nanopores because *profile height both in glasses and GMN is of the same order* [70]. One can see from Fig. 5.2 the height of the profile imprinted on the glass surface increases up to 45-50 nm. Such a height is reached at the groove widths of 500-600 nm. The relation between width and height exists owing to the concurrence of normal and lateral components of electric field in the vicinity of a groove and consequent interplay between normal and lateral ionic fluxes (see paper **VI**) and the diffusional smearing is also responsible for the hump width-height relation.

Processes of the surface profile formation and nanoparticle dissolution are tightly connected via local electric fields formed in the course of the ions redistribution. Nevertheless, the formation of surface profile humps 100 nm width does not correspond to the modulation of nanoparticle concentration on the same scale. To obtain information about nanoparticle distribution on such scales we resorted to SNOM technique. Near-field optical microscopy measurements were performed using an aperture-type SNOM (AIST-NT CombiScope Scanning Probe Microscope with optical fiber probe) in transmission mode [81]. The setup allowed us to perform the scanning both in contact with the surface and at constant height above the surface.

Structures imprinted both in GMN and in virgin glass were tested at the wavelengths of 633, 532, and 405 nm. Since the plasmon resonance in the GMN is centered at 420 nm, the optical density of the GMN increases with the decrease of the laser wavelengths. The electric field vector of the incident light was polarized perpendicular to the imprinted stripes. The signal cross-section was obtained after averaging of the 2D scanning data over the stripe length. The results for GMN sample are shown in Fig. 5.2.

In the virgin glass, the electric field intensity modulation is of the order of $\sim$ 3%, while the electric field structure is similar for all the wavelengths. The amplitude increases with the increase of stripe width becoming constant at the stripe of 500-600 nm width. Two physical mechanisms can contribute to the observed modu-

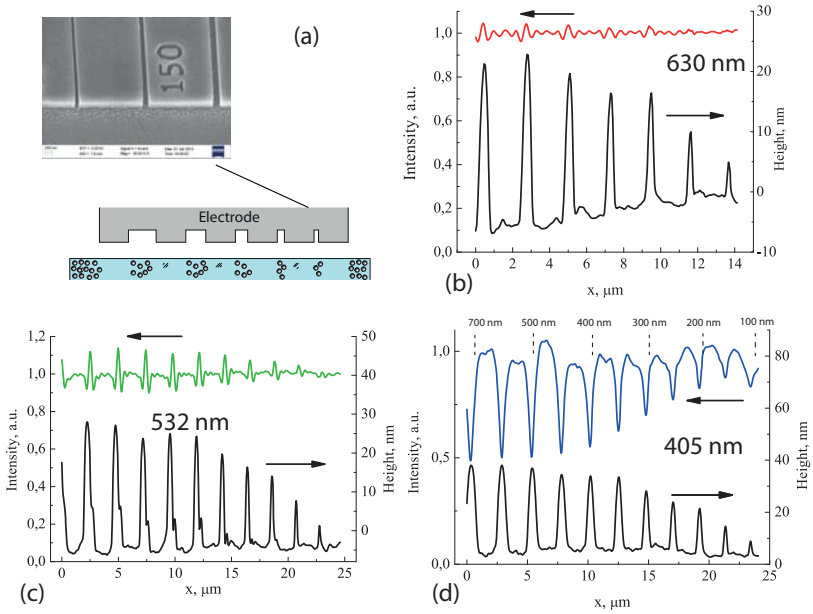

Figure 5.2: (a) SEM image of 100, 150, and 200 nm grooves on anode surface; the scheme of imprinting process. Transmitted intensity distribution at 633 nm (b), 532 nm (c), and 405 nm (d) wavelengths; AFM surface profile is shown for each measurement.

lation of the light intensity. The first possible mechanism is the interference of incident wave with the wave scattered by the surface humps. The second mechanism of the intensity modulation may be associated with the phase shift accumulated due to the refractive index change in the poled glass that can be as high as $\Delta n \approx -(0.03 - 0.09)$ [82]. The performed calculations showed that at the obtained poling depths of about 1 μm the accumulated phase shift is not sufficient to produce the observed modulation of the optical signal. On the other hand, the modeling of light scattering with COMSOL Multyphisics package for 10-50 nm humps on a glass surface revealed that the intensity modulation can be as high as several percents. Thus, most likely the scattering mechanism is responsible for the observed optical signal modulation in glass sample.

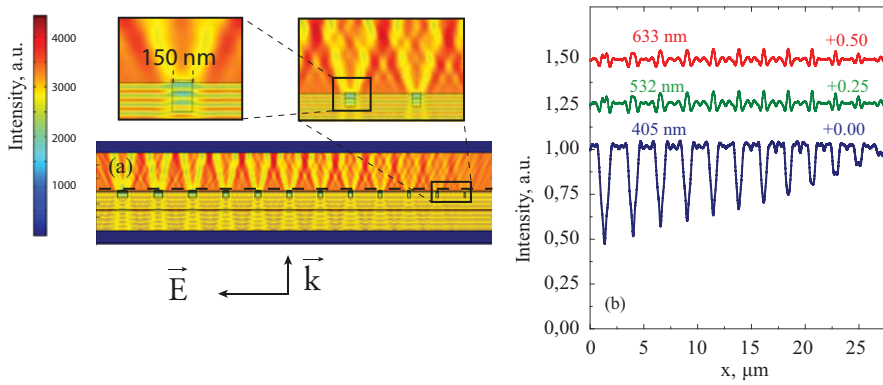

Figure 5.3: (a) 2D plot of the calculated light intensity in transmission geometry at 405 nm wavelength; (b) Calculated electric field distribution at different wavelengths.

The SNOM measurements in GMN sample at red and green wavelengths also showed light intensity modulation with maximal amplitude of about 10%. The amplitude increases with the increase of stripe width becoming constant at the width of 500-600 nm. No significant difference in the intensities in the contact and lifted regime was observed. The modulation has the same origin as that in virgin glass because the optical absorption of GMN is low at the red and green wavelengths.

Maximal transmitted ligth modulation of up to 50% was observed at the wavelength that corresponded to the SPR in silver nanoparticles. In contrast to the irradiation with red and green light, we observed decrease of the light intensity at the wavelength of 405 nm. This confirmed that nanoparticles in the unpoled areas survived. One can observe from Fig. 5.2 that the narrower is the line, the lower is the amplitude of the intensity modulation. One can also conclude that the best spatial resolution was of order of 150 nm because the image of the 100 nm thin line was smeared after averaging of 2D data.

To verify the obtained experimental results we performed FEM modeling using COMSOL Multyphisycs package. In the calculations, we employed the Maxwell Garnett effective medium ap-

proach with filling factor f = 0.01 to model optical parameters of the GMN. The depth of the nanocomposite layer used in the calculations was 300 nm. One can observe from Fig. 5.3 that obtained light intensity distribution in the nanocomposite well corresponds to the experimental data. It is important to stress that according to the modeling results nanoparticle concentration is nearly the same we can conclude that in the 150 nm wide imprinted stripe as in the initial GMN sample. Thus, the obtained minimal imprinted linewidth proves the applicability of EFAD technique for fabrication nanoscale GMN-based plasmonic and photonics components.

5.2 GLASS POLING WITH PERIODIC ELECTRODE

Imprinting technique can be used to fabricate optical structures in silica based glasses. Last years glass poling have been of high scientific interest because of its applicability in nonlinear optics [41], electrooptics [47], integrated optics [83], and sensoric [84]. The methodology of glass imprinting is similar to that of GMN. The difference is that in the case of glass imprinting, the phase modulation is caused by the refractive index change is observed, while in the GMN imprinting, where amplitude modulation dominates. Though the obtained refractive index change is small ($\Delta n \approx 0.03 - 0.09$ [82]) the non-zero second order nonlinearity of the periodically poled regions can be employed in nonlinear optical and photonic devices. However for possible nonlinear optical and photonics applications it is crucial to know the achievable spatial resolution of electric field imprinting. The detailed modeling of silica glass imprinting with periodical electrode was carried out in paper **VI**. It was established that there exists a set of poling parameters (time, voltage) that provide optimal photonic structures of given spatial dimensions in the subanodic region. These optimal imprinting conditions are determined by the interplay of diffusion and drift components of the charge flux in the course of glass poling with profiled anode.

6 GMN based diffraction gratings

Since the optical properties of GMN are mainly governed by the SPR, it also strongly influences characteristics of GMN based photonic structures and, in particular, diffraction gratings fabricated using GMN. In this Thesis we consider optical properties of 1D diffraction grating based on GMN.

6.1 EFFECTIVE MEDIUM APPROACH

Optical properties of composite media can be described using effective medium theory approach [85] that implies the homogenization of composite by introducing effective dielectric constant ε_{eff}. It can be defined from the following constitutive equation:

$$\langle D \rangle = \varepsilon_{eff} \langle E \rangle ,$$

where $\langle E \rangle$ and $\langle D \rangle$ are mean electric field strength and electric displacement. One of the key parameters that determines the effective constant ε_{eff} is filling factor or, the same, nanoparticle volume fraction

$$f = \frac{V_{nanoparticles}}{V_{composite}}.$$

Depending on the structure of nanocomposite its optical properties can be described by different effective medium theories. One of the common approaches is based on Bruggeman theory [86] that considers two-component composite with indistinguishable phases, i.e. the structure of nanocomposite does not change after swapping the phases. This theory well describes composites with filling factor around $f \sim 0.5$, however it can not be employed to describe the optical properties of the metal-dielectric nanocomposite in the vicinity

of SPR [87]. Since one may expect that most significant effects in GMN-based structures take place when the frequency of the light wave is close to the SPR, in this Thesis, we will use Maxwell Garnett (MG) approach [88], which is valid in the whole spectral range. In contrast to the Bruggeman thory, the MG theory can be employed only at small filling factor, i.e. when the GMN is far from percolation threshold and when the nanoparticle diameter radius R is much less than the average distance between nanoparticles, which in its turn is much less than the light wavelength λ, $R \ll a \ll \lambda$. However experimentally measured bounds of Maxwell Garnett theory applicability are smeared. The filling factor range $f < 0.2$ and $f > 0.8$ ensures correctness of MG theory, but in the further calculations we consider fill factor up to 0.3 to illustrate the basic properties of GMN based gratings. In the framework of the MG theory, the

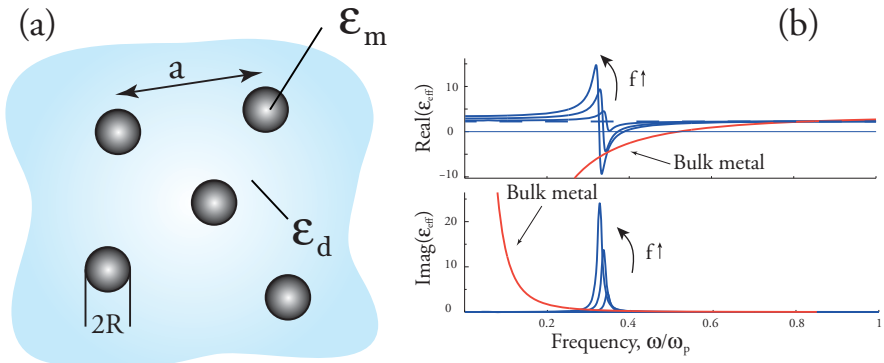

Figure 6.1: (a) Glass metal nanocomposite. (b) Real and imaginary part of ε_{eff} for pure glass (dashed line) and filling factors $f = 0.03, 0.09, 0.15$ (blue lines) and for bulk metal (red line).

effective dielectric permittivity is described by the following equation:

$$\varepsilon_{eff} = \varepsilon_d \frac{\varepsilon_m + 2\varepsilon_d + 2f(\varepsilon_m - \varepsilon_d)}{\varepsilon_m + 2\varepsilon_d - f(\varepsilon_m - \varepsilon_d)}, \tag{6.1}$$

where ε_m and ε_d are permittivities of metal nanoparticles and glass matrix, respectively (see fig. 6.1) .

By using Drude model (2.1) for dielectric permittivity of metal the effective constant of the GMN (6.1) can be presented in the following form:

$$\varepsilon_{eff}(\omega) = \varepsilon_{eff}^{\infty} \frac{\omega^2 - \omega_L^2 + i\gamma\omega}{\omega^2 - \omega_T^2 + i\gamma\omega}, \tag{6.2}$$

where

$$\varepsilon_{eff}^{\infty} = \varepsilon_d \frac{1+2f}{1-f},$$

$$\omega_T^2 = \omega_p^2 \frac{1+2f}{\varepsilon_\infty + 2\varepsilon_d + 2f(\varepsilon_\infty - \varepsilon_d)}, \tag{6.3}$$

and

$$\omega_L^2 = \omega_p^2 \frac{1-f}{\varepsilon_\infty + 2\varepsilon_d - f(\varepsilon_\infty - \varepsilon_d)}. \tag{6.4}$$

Frequencies (ω_L) and (ω_L) are usually referred to as longitudinal and transversal frequencies, respectively. The dielectric permittivity in the form (6.2) is typical when the optical properties of the medium is governed by a strong resonance [34], e.g. in molecular gases, ionic crystals, dye doped solids, and semiconductors. In GMN, this resonance is associated with localized surface plasmon, i.e. dipole oscillations of free electron gas in metal nanoparticles. It is worth noting that if the nanoparticle circumference is comparable or larger than the wavelength, higher-order multipoles (quadrupole, octapole, etc.) strongly influence its polarizability. In such a case the equation for the effective permittivity (6.2) should be complemented with extra terms of similar structure, which describe contributions of these higher-order resonances [36].

At $f = 1$ equation (6.2) turns into (2.1) thus describing permittivity of pure metal as $\omega_T \to 0$ and $\omega_L \to \omega_p/\sqrt{\varepsilon_\infty}$. For low nanoparticle concentration $\omega_T \to \omega_L$ as $f \to 0$. The evolution of real and imaginary parts of effective dielectric permittivity of GMN with different filling factors is shown in fig. 6.1 (b) for silver nanoparticles ($\varepsilon_\infty = 3.9$, $\omega_p = 9.1$ eV, $\tau = 30$ fs [89]) in silicate glass with $\varepsilon_d = 2.25$. The permittivity of bulk silver is also shown.

The damping factor γ determines electron scattering frequency $1/\tau$ and in bulk metal it is mainly governed by the lattice scattering frequency $1/\tau_l$. However, in a metal nanoparticle, the electron scattering on the nanoparticle surface also should be accounted [85] resulting in

$$\gamma = \frac{1}{\tau} = \frac{1}{\tau_l} + A\frac{v_f}{R},$$

where v_f is Fermi velocity and A is phenomenological factor of order of 1. In small nanoparticles, the surface scattering dominates over lattice scattering giving rise to the dependence of the effective permittivity on the radius R. However, in this Chapter, we will neglect this dependence that is acceptable for nanoparticles of $R >$ 5 nm.

6.2 OPTICAL PROPERTIES OF GMN BASED GRATINGS

In this section we discuss the 1D GMN based gratings to analyze how GMN optical characteristics influence optical properties of the grating. In order to reveal this we consider binary gratings with duty factor 0.5 (see Fig. 6.2) and normal incidence of TE and TM plane waves.

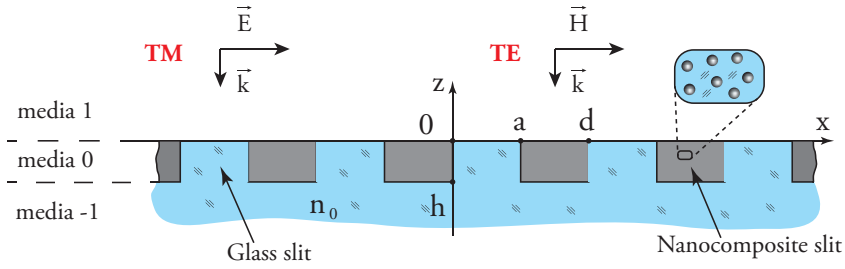

Figure 6.2: Structure of diffraction grating considered in this Thesis.

We start from the case of gratings with period much longer than the light wavelength, $d \gg \lambda$.

6.2.1 Long period limit $d \gg \lambda$

When the light wavelength is much shorter than grating period d one can employ the thin element approximation [90] assuming that electromagnetic field inside the grating layer 0 (see Fig. 6.2) can be treated as a plane wave. Such an assumption is valid if lateral energy flux is much less than normal one, i.e. when $h/d \ll 1$, where h is the grating height. The transmitted and reflected waves at $z = -h$ can be presented in the following form:

$$E_T(x,-h) = T(x)E_I(0), \qquad E_R(x,-h) = R(x)E_I(0), \tag{6.5}$$

where $T(x)$ and $R(x)$ are grating transmission and reflection coefficients and $E_I(z) = E_0 \exp(ikz)$ is the incident wave. Here we drop time dependence $\sim \exp(-i\omega t)$. Note that for normal incidence there is no difference between TE and TM polarizations, for they have the same Fresnel coefficients. The transmission coefficient can be written as

$$T(x) = t_{1,-1}(x) \exp\left(i\phi(x)\right) \exp\left(-\alpha(x)\right),$$

here $t_{1,-1}(x) = t_{1,0}(x)t_{0,-1}(x)$ is Fresnel transmittance coefficient from media 1 to -1, $\phi(x)$ is the phase shift that wave accumulates while propagating through the 0 region, $\alpha(x)$ is the attenuation coefficient in layer 0. Introducing complex refractive index $n(x) = n'(x) + in''(x)$ that is periodic function we can write

$$\phi(x) = k(n'(x) - n_0)H(x), \qquad \alpha(x) = kn''(x)H(x).$$

$H(x)$ is periodic profile function that in the case of grating presented in the fig. 6.2 equals to

$$H(x) = \begin{cases} 0, & 0 < x \le a \\ h, & a < x \le d \end{cases}$$

Similarly to (6.5) we can write the expression for the reflection coefficient

$$R(x) = r_{10}(x), \tag{6.6}$$

where $r_{10}(x)$ is Fresnel reflection coefficient. It is necessary to note that in the Eqs. (6.5,6.6) we do not take into account multiple reflections from the regions boundaries, otherwise, for example, reflection coefficient should be written as

$$R(x) = r_{10}(1 + r_{0,-1}t_{0,1}\exp(i2\phi(x))\exp(-2\alpha(x)) + ...)$$

forming a series with rapidly decreasing components.

Since, $T(x)$ and $R(x)$ are periodic function, the electric field of the transmitted and reflected waves can be decomposed into the Fourier series as the following:

$$\begin{aligned} E_T(x,z) &= T(x)E_I(0)\exp(in_0kz) = \\ &= E_0\textstyle\sum_{-\infty}^{\infty} T_m \exp(in_0kz + in_0mKx), \\ K &= \frac{2\pi}{d}. \end{aligned} \tag{6.7}$$

The diffraction field in reflected rays has similar form

$$\begin{aligned} E_R(x,z) &= R(x)E_I(0)\exp(in_0kz) = \\ &= E_0\sum_{-\infty}^{\infty} R_m \exp(ikz + imKx). \end{aligned} \tag{6.8}$$

Each term in the sums (6.7)–(6.8) relates to m-th diffraction order. The diffraction efficiency of m-th transmitted and reflected orders can be expressed as $\theta_m = |T_m|^2$ and $\eta_m = |R_m|^2$, respectively.

The transmittance and reflectance spectra of the GMN grating with high filling factor of $f = 0.3$ is shown in fig. 6.3 (a) for zero and first diffraction orders. The dielectric parameters of silver were taken from Johnson and Christy [91].

One can see that spectral properties of GMN gratings are mainly governed by GMN dielectric permittivity, which is also shown in Fig. 6.3. The longitudinal $\lambda_L = 2\pi c/\omega_L$ and transversal $\lambda_T = 2\pi c/\omega_T$ wavelengths divide the considered spectral region into three bands. In the first ($\lambda \leq \lambda_L$) and the third ($\lambda > \lambda_T$) bands the real part of dielectric permittivity is positive, and imaginary part is small. This corresponds to *phase grating* regime, in which transmittance is determined by the phase difference accumulated by the

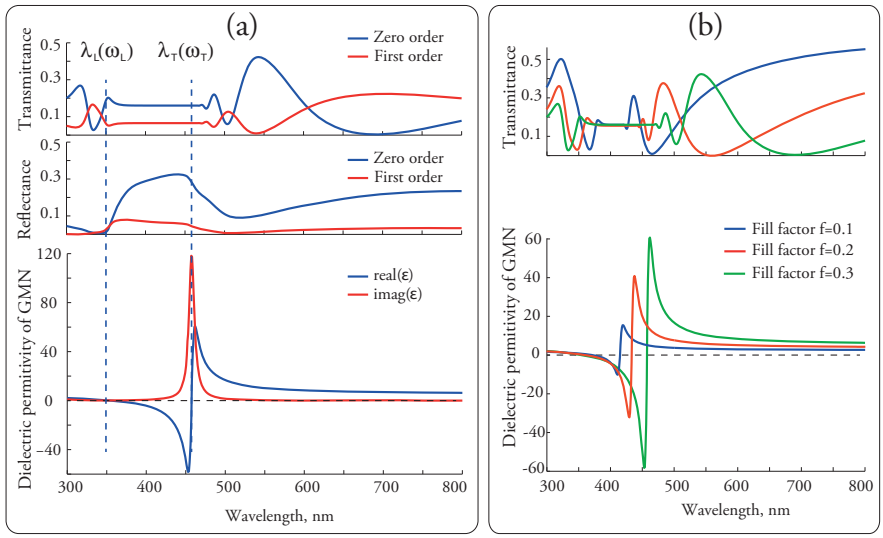

Figure 6.3: Properties of GMN grating (see Fig. 6.2) with the following parameters: $h = 300$ *nm,* $a/d = 0.5$*,* $n_0 = 1.5$*. (a) Reflectance and transmittance spectra at the GMN filling factor of* $f = 0.3$ *. (b) Zero-order transmittance spectra at the GMN filling factor of* $f = 0.1, 0.2, 0.3$*. Spectra of the GMN permittivity are also shown.*

incident wave after transmission through GMN slits. The second band ($\lambda_L < \lambda \leq \lambda_T$) corresponds to negative permittivity region with high losses at the resonance frequency. In this band, the incident light is mainly reflected from the GMN slits (see reflectance spectra in Fig. 6.3 (a)). Such a reflectance band often is referred in the literature as *reststrahlen band* [92]. It corresponds to the band of constant transmission as the transmitted light is passing mainly through glass slits. In this band, since the transmission is determined by light passed through glass slits, the diffractive grating manifests itself as an *amplitude grating*. The width $\Delta\omega_{rfl}$ of the reflectance band depends on filling factor. This can be seen from fig. 6.3 (b) where transmission spectra for different filling factors are shown. In the frames of the Drude model, the spectral width of this band is determined by $\Delta\omega_{rfl} = \omega_L - \omega_T$, and for low filling factors

$f \ll 1$ it gives:

$$\omega_{rfl}(f) = \frac{9}{2}\frac{\varepsilon_d \omega_p}{\sqrt{\varepsilon_\infty + 2\varepsilon_d}} f.$$

Thus the reflectance band of GMN grating can be changed by tuning the filling factor.

6.2.2 Gratings with $d \sim \lambda$

The considered case of long period gratings gives a clear picture of how nanocomposite microstructure influences the diffraction properties. However, for photonics applications gratings with period comparable with wavelength and even subwavelength gratings are more relevant. Description of the light diffraction by gratings with period and height comparable with light wavelength ($d \sim \lambda$ and $h \sim \lambda$) requires solution of the rigorous diffraction problem. For that we will imply Fourier Modal Method (FMM) [90,93–95] that allows construction of the rigorous solution of the plane wave diffraction problem on binary grating. Considering the case of TE polarization the diffraction problem is reduced to the solution of Helmholtz equation for y-component of electric field $E_y(x,z)$

$$\frac{\partial^2 E_y(x,z)}{\partial z^2} + \frac{\partial^2 E_y(x,z)}{\partial x^2} + \varepsilon(x,z) k_0^2 E_y(x,z) = 0 \qquad (6.9)$$

with corresponding boundary conditions at the grating surfaces. We will look for the solution in the upper and lower regions (region +1 and -1 respectively) in the form of Rayleigh expansion:

$$\begin{aligned} E_y^+ &= E_0 \exp(ik_x^{inc} x)\exp(-ik_z^{inc} z) + \sum_{m=-\infty}^{\infty} R_m \exp(ik_{xm} x)\exp(ik_{zm}^+ z), \\ E_y^- &= \sum_{m=-\infty}^{\infty} T_m \exp(ik_{xm} x)\exp(-ik_{zm}^- z), \end{aligned} \qquad (6.10)$$

where the first term is the E_y^+ corresponds to illuminating the grating incident plane wave with wave vector $\boldsymbol{k}_{inc} = (k_x^{inc}, -k_z^{inc})$ and amplitude E_0. The sums in the expressions for E_y^+ and E_y^- correspond to reflected and transmitted diffraction orders with amplitudes R_m and T_m, respectively. Applying the pseudoperiodicity

condition we can conclude that

$$k_{xm} = k_x^{inc} + mK, \text{ where } K = \frac{2\pi}{d}$$

is Bragg vector and m is diffraction order. In the grating layer 0 the solution can be obtained after devision of variables resulting in

$$E_y^0(x,z) = \sum_{m=-\infty}^{\infty} \exp(ik_{xm}x)\left(c^+ \exp(i\gamma z) + c^- \exp(-i\gamma z)\right),$$

where γ are propagation constants within the grating layer. Expressing magnetic field component of TE mode H_x via E_y we can write down the boundary conditions:

$$\begin{aligned} E_y^+(x,0+) &= E_y^0(x,0-) \qquad H_x^+(x,0+) = H_x^0(x,0-) \\ E_y^0(x,-h+) &= E_y^-(x,-h-) \qquad H_x^0(x,-h+) = H_x^-(x,-h-). \end{aligned}$$

This system gives us an eigen value problem that allows finding a set of propagation constants $\{\gamma_k\}$. Thus we can obtain the solution for the light amplitude within the grating layer in the following form:

$$E_y^0(x,z) = \sum_{k=-\infty}^{\infty} \sum_{m=-\infty}^{\infty} A_{nk}\left(c_k^+ \exp(i\gamma_k z) + c_k^- \exp(-i\gamma_k z)\right) \exp(ik_{xm}x),$$

where A_{nk} is matrix formed by eigen vectors of the considered problem. The required mode amplitudes T_m, R_m, c_k^+, c_k^- can be found with S-matrix algorithm [93].

The case of TM-polarization can be considered in the same manner as the TE case, for the basic equation has similar form:

$$\frac{\partial}{\partial z}\left(\frac{1}{\varepsilon(x,z)}\frac{\partial H_y(x,z)}{\partial z}\right) + \frac{\partial}{\partial x}\left(\frac{1}{\varepsilon(x,z)}\frac{\partial H_y(x,z)}{\partial x}\right) + k_0^2 H_y(x,z) = 0. \tag{6.11}$$

However, implementation of FMM for TM polarized illumination requires special regularization to avoid numerical instability [94].

In this section we consider the results of the numerical analysis for grating with period $d = 800$ nm and height $h = 200$ nm (see Fig. 6.3). In contrary to long period gratings considered in previous section, the diffraction by the submicron grating is polarization dependent even at normal incidence. The transmittance spectra of the first order obtained from exact solution of diffraction problem are shown in fig. 6.4 (a) for TE polarization and different GMN filling factors.

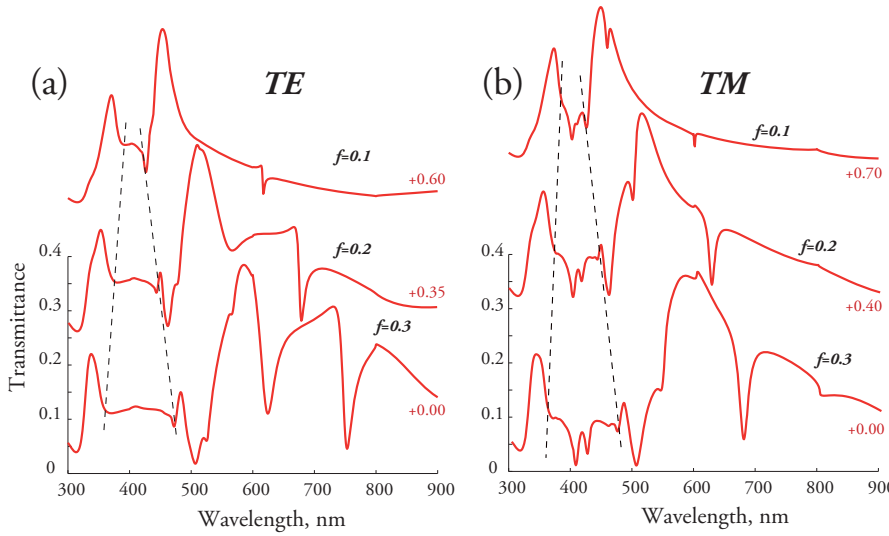

Figure 6.4: Transmission spectra of first diffraction order of TE (a) and TM (b) polarized wave obtained with FMM method. Grating parameters $d = 800$ nm, $h = 200$ nm, $a/d = 0.5$, $n_0 = 1.5$. Optical constants are taken from Johnson & Christy [91].

One can see that similarly to the case of long period grating there exists a reflectance band (constant transmission) that gets wider with filling factor increase. This corresponds to amplitude grating mode. The distribution of y-component of electric field amplitude $|E_y|$ is shown in Fig. 6.5 at wavelengths $\lambda = 400$ nm for $f = 0.2$ and TE polarization. One can see that (Fig. 6.5 a) almost all the light that incidences the nanocomposite slit $0 < x \leq a$ scatters back in accordance with calculated reflectance spectra in Fig. 6.4.

Meanwhile the glass slit $a \leq x \leq d$ reflects light only partially and the other part is being transmitted in the region -1.

The long ($\lambda > \lambda_T$) and short ($\lambda < \lambda_L$) wavelength regions correspond to phase grating regime. At 520 nm the nanocomposite slits become transparent, and light passes through. Corresponding interference pattern in the transmitted field can be observed (Fig. 6.5 b). However in contrast to the case of long period gratings we observe sharp deeps in the transmission spectra. It is worth noting that the GMN refractive index is high in the spectral region $\lambda > \lambda_T$. Indeed, it has been shown that in symmetric homogenious ionic crystal slabs with dispersion law (6.2) there exists waveguiding mode as refractive index is high [96–98]. This indicates that the sharp deeps in Fig. 6.4 may be associated to resonant excitation of waveguide modes propagating in the grating layer (Fano resonances). Such a conclusion is supported by the image of the field distribution in the vicinity of resonance ($\lambda = 676$ nm) shown in Fig. 6.5 (c). One can see that the wave is mainly localized in the grating layer that confirms generation of waveguide mode.

TM polarization spectra have structure similar to TE case (see fig. 6.4 (b)) that is they demonstrate the reflectance band in the region of negative dielectric permittivity as well as the excitation of waveguide modes. However, in the reflectance band there exist the deeps that were not observed in the TE polarization. These deeps may be associated with localized resonances of individual nanocomposite stripes having negative real component of effective dielectric permittivity. The field distribution is shown in Fig. 6.5 (d, e). We should stress that in the region $\lambda_L < \lambda < \lambda_T$ surface polariton modes may also propagate in the grating layer as negative permittivity is the main condition of their existence [36], and their contribution into total diffraction spectrum is possible.

6.2.3 Gratings with $d \ll \lambda$

The limit of long wavelengths, i.e. at $\lambda \gg d$ implies that no diffraction is observed. Materials with subwavelength structuring are

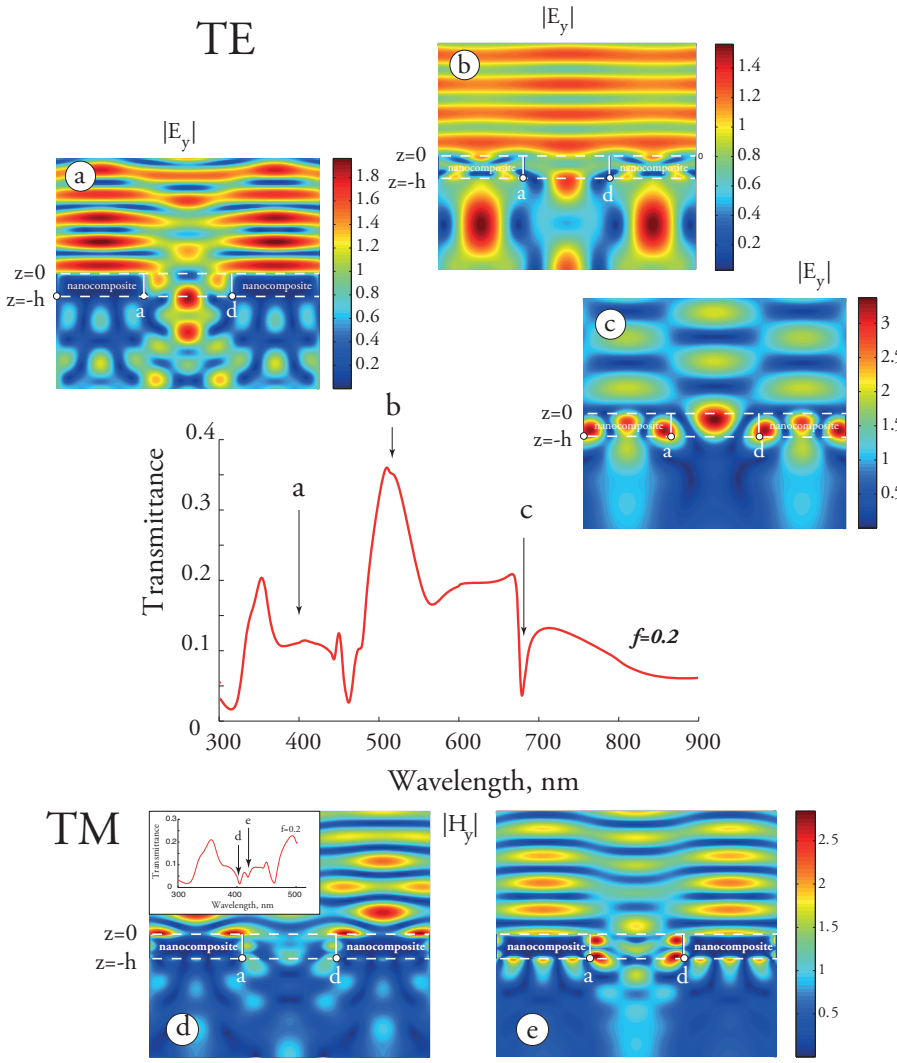

Figure 6.5: Spatial distribution of the electric field amplitude for TE-polarized incident wave at 400 nm (a), 520 nm (b), 676 nm (c). Spatial distribution of the magnetic field amplitude for the TM polarized incident wave at 404 nm (e) and 418 nm (d). TE and TM transmittance spectra are also shown for GMN with $f = 0.2$.

called *metamaterials* and nowadays attract much interest in photonics and nanoelectronics [99].

We consider light propagation through based on GMN subwavelength grating based on GMN using two approaches. The first one uses rigorous FMM method that gives exact solution of the problem. The second is approximate solution that is based on homogenization of grating layer. Since the light wavelength is much longer than the grating period we can implement effective medium approach. Thus, the considered grating consists of nanocomposite slits which can be described with MG theory and glass slits according to Fig. 6.2. Such a double composite nature of the grating imposes the restriction on the minimum size of the grating period. Specifically, the grating features should be much larger than the distance between neighbour nanoparticles. Applying this "double" homogenization procedure we can write effective permittivity of grating layer for TE and TM polarization (see Fig. 6.6) :

$$\varepsilon_{TE} = g\varepsilon_1 + (1-g)\varepsilon_2, \qquad \text{for TE polarization}$$

and

$$\frac{1}{\varepsilon_{TM}} = \frac{g}{\varepsilon_1} + \frac{(1-g)}{\varepsilon_2}, \qquad \text{for TM polarization,}$$

where $\varepsilon_1 = \varepsilon_{eff}(f)$, $\varepsilon_2 = \varepsilon_d$, and $g = a/d$ is filling factor of grating. Simple algebra allows us to find that the effective permittivity of the grating has the same form as (6.1). Neglecting losses $\gamma = 0$ we can write it down:

$$\varepsilon_{TE} = \varepsilon_{TE}^{\infty}(f,g)\frac{\omega^2 - \hat{\omega}_L^2(f,g)}{\omega^2 - \omega_T^2(f)}, \tag{6.12}$$

$$\varepsilon_{TM} = \varepsilon_{TM}^{\infty}(f,g)\frac{\omega^2 - \omega_L^2(f)}{\omega^2 - \hat{\omega}_T^2(f,g)}, \tag{6.13}$$

where $\omega_T(f)$ and $\omega_T(f)$ are defined by (6.3) and (6.4). The parameters $\hat{\omega}_T(f,g)$ and $\hat{\omega}_L(f,g)$ are new characteristic frequencies that depend on two filling factors because g and f together equally define the amount of metal in the grating layer.

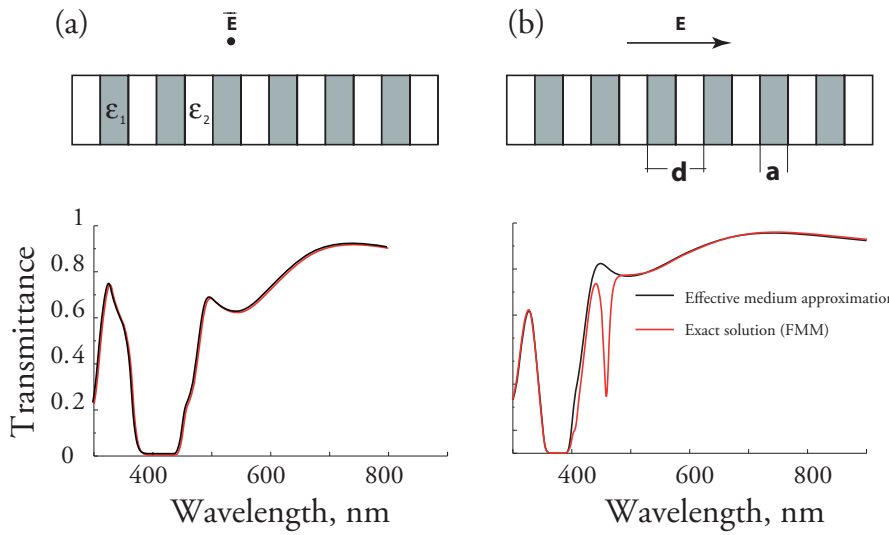

Figure 6.6: Transmittance spectra of subwavelength grating with period $d = 30$ nm, $g = a/d = 0.5$, $f = 0.3$, and $h = 200$ nm for TE (a) and TM (b) polarization obtained in the frames of effective medium approach and with rigorous FMM solution.

Having expression for ε_{TE} and ε_{TM} we used simple T-matrix method to simulate reflectance and transmittance of normally incident light through grating layer with period $d = 30$ nm, $g = 0.5$ and $f = 0.3$. The results of the simulation are shown in Fig. 6.6 with black line. One can see that at $d \ll \lambda$ there exists zero transmission region, in which effective permittivity of the double-composite media is negative and which corresponds to the reflection band discussed in previous sections. Beyond these region, the transmittance is governed by interference of the incident wave and the waves reflected from grating layer planes $z = 0$ and $z = -h$.

The results of the exact solution obtained with FMM method are also shown. One can clearly see that in the case of TE polarization both approaches give identical results. However, in the case of TM polarization local resonances in the grating layer, which can not be predicted by the effective medium theory, essentially influence the transmittance. In this case the describing the periodic structures

with effective medium approach is not valid.

The mismatch between effective model approach and exact solution in analysis of periodic structures has been discussed actively last decade. This discrepancy originates from excitement of surface waves in the grating layer that gives contribution in the transmission spectrum. One of the most known examples that has the similar nature is extraordinary transmission of periodic subwalength apertures in metal films [100, 101]. The generation of surface plasmon waves is responsible for enhanced transmission effects. Mode analysis of layered metal-dielectric structures [102] also exhibit significant difference between exact solution and solution based on the effective medium approach. The discrepancy shown in Fig. 6.6 can be related to propagation of plasmonic modes in the gap between grating slits. Thus one of the alternative descriptions can be based on the consideration of grating as a system of interacting plasmonic waveguides in the direction normal to the surface.

Thus, we can conclude that optical properties of GMN-based structures strongly depend on the nanoparticle concentration. This additional degree of freedom gives a powerful tool to control diffraction properties of GMN gratings.

7 Conclusions

This Thesis is focused on joint electric field and temperature effects in glasses and glass-metal nanocomposites and on the fabrication of subwavelength planar optical structures via electric field assisted dissolution of metal nanoparticles in GMN. Optical properties of GMN-based photonic structures have been examined both theoretically and experimentally.

The main results obtained in the presented work are the following:

- Modeling of soda-lime glass poling was performed with the account for low mobile ions drift. Both analytical and numerical results showed a good coincidence with experimental data reported in the literature.

- By using the proposed models of the glass and GMN poling the theory of the EFAD process was developed. Performed experiments on EFAD assisted bleaching showed that the developed theory well describes the experimental data and reveals main factors that influence dissolution of metal nanoparticles in silicate glass.

- Modeling of the electric field assisted imprinting on the glass surface was performed. It was demonstrated that there exists optimal set of imprinting conditions allowing one to fabricate a planar periodic structure with prescribed parameters.

- Subwavelength planar optical structures were fabricated via EFAD assisted bleaching of silver-based GMN fabricated via ion exchange process followed by hydrogen silver reduction.. Near field optical microscopy measurements confirmed that the EFAD technique enables fabrication of structures with feature size as small as 150 nm.

- Theoretical study of GMN-based diffraction gratings was performed. We showed that the these gratings exhibit either amplitude or phase behavior depending on the nanoparticles volume fraction and the SPR frequency. This gives additional degree of freedom for engineering diffraction patterns.

We can conclude that obtained results demonstrate high application potential of GMN for optics, photonics, and plasmonics. The theoretical and experimental findings presented in Thesis open a route for simple, precisely controllable, and cost-effective fabrication of planar structures with subwavelength resolution.

Bibliography

[1] A. Moroz, "Three-Dimensional Complete Photonic-Band-gap Structures in the Visible," *Physical Review Letters* **83,** 5274–5277 (1999).

[2] W. Zhang, X. Lei, Z. Wang, D. Zheng, W. Tam, C. Chan, and P. Sheng, "Robust Photonic Band Gap from Tunable Scatterers," *Physical Review Letters* **84,** 2853–2856 (2000).

[3] P. T. Guerreiro, S. Ten, N. F. Borrelli, J. Butty, G. E. Jabbour, and N. Peyghambarian, "PbS quantum-dot doped glasses as saturable absorbers for mode locking of a Cr:forsterite laser," *Applied Physics Letters* **71,** 1595 (1997).

[4] A. M. Malyarevich, K. V. Yumashev, and A. A. Lipovskii, "Semiconductor-doped glass saturable absorbers for near-infrared solid-state lasers," *Journal of Applied Physics* **103,** 081301 (2008).

[5] C. M. Soukoulis, "Bending Back Light: The Science of Negative Index Materials," *Optics and Photonics News* **17,** 16 (2006).

[6] N. P. Johnson, A. Z. Khokhar, H. M. Chong, R. M. Rue, T. J. Antosiewicz, and S. McMeekin, "A review of size and geometrical factors influencing resonant frequencies in metamaterials," *Opto-Electronics Review* **14,** 187–191 (2006).

[7] D. Schurig, J. J. Mock, B. J. Justice, S. A. Cummer, J. B. Pendry, A. F. Starr, and D. R. Smith, "Metamaterial electromagnetic cloak at microwave frequencies," *Science* **314,** 977–80 (2006).

[8] M. Dubiel, H. Hofmeister, and E. Wendler, "Formation of nanoparticles in soda-lime glasses by single and double ion implantation," *Journal of Non-Crystalline Solids* **354,** 607–611 (2008).

[9] P. Chakraborty, "Metal nanoclusters in glasses as non-linear photonic materials," *Journal of Materials Science* **33,** 2235–2249 (1998).

[10] A. Chiasera, M. Ferrari, M. Mattarelli, M. Montagna, S. Pelli, H. Portales, J. Zheng, and G. Righini, "Assessment of spectroscopic properties of erbium ions in a soda-lime silicate glass after silver–sodium exchange," *Optical Materials* **27,** 1743–1747 (2005).

[11] G. Sun, J. B. Khurgin, and R. A. Soref, "Practical enhancement of photoluminescence by metal nanoparticles," *Applied Physics Letters* **94,** 101103 (2009).

[12] Y. Chen, L. Karvonen, A. Saynatjoki, C. Ye, A. Tervonen, and S. Honkanen, "Ag nanoparticles embedded in glass by two-step ion exchange and their SERS application," *Optical Materials Express* **1,** 164–172 (2011).

[13] V. V. Zhurikhina, P. N. Brunkov, V. G. Melehin, T. Kaplas, Y. Svirko, V. V. Rutckaia, and A. A. Lipovskii, "Self-assembled silver nanoislands formed on glass surface via out-diffusion for multiple usages in SERS applications.," *Nanoscale Research Letters* **7,** 676 (2012).

[14] A. Stalmashonak, A. Abdolvand, and G. Seifert, "Metal-glass nanocomposite for optical storage of information," *Applied Physics Letters* **99,** 201904 (2011).

[15] O. Deparis, P. G. Kazansky, A. Abdolvand, A. Podlipensky, G. Seifert, and H. Graener, "Poling-assisted bleaching of metal-doped nanocomposite glass," *Applied Physics Letters* **85,** 872 (2004).

[16] I. C. Carvalho, F. P. Mezzapesa, P. G. Kazansky, O. Deparis, M. Kawazu, and K. Sakaguchi, "Dissolution of embedded gold nanoparticles in sol–gel glass film," *Materials Science and Engineering: C* **27,** 1313–1316 (2007).

[17] A. A. Lipovskii, V. G. Melehin, and V. D. Petrikov, "Electric-field-induced bleaching of ion-exchanged glasses containing copper nanoparticles," *Technical Physics Letters* **32,** 275–277 (2006).

[18] A. Abdolvand, A. Podlipensky, S. Matthias, F. Syrowatka, U. Gösele, G. Seifert, and H. Graener, "Metallodielectric Two-Dimensional Photonic Structures Made by Electric-Field Microstructuring of Nanocomposite Glasses," *Advanced Materials* **17,** 2983–2987 (2005).

[19] a. a. Lipovskii, M. Kuittinen, P. Karvinen, K. Leinonen, V. G. Melehin, V. V. Zhurikhina, and Y. P. Svirko, "Electric field imprinting of sub-micron patterns in glass-metal nanocomposites.," *Nanotechnology* **19,** 415304 (2008).

[20] V. Janicki, J. Sancho-Parramon, F. Peiró, and J. Arbiol, "Three-dimensional photonic microstructures produced by electric field assisted dissolution of metal nanoclusters in multilayer stacks," *Applied Physics B* **98,** 93–98 (2009).

[21] P. Brunkov, V. Goncharov, V. Melehin, A. Lipovskii, and M. Petrov, "Submicron Surface Relief Formation Using Thermal Poling of Glasses," *e-Journal of Surface Science and Nanotechnology* **7,** 617–620 (2009).

[22] H. Takagi, S.-i. Miyazawa, M. Takahashi, and R. Maeda, "Electrostatic Imprint Process for Glass," *Applied Physics Express* **1,** 024003 (2008).

[23] Z. Zou, Q. Wang, X. Chen, and S. Qu, "Direct evidence for electric field assisted dissolution of Au nanoparticles on glass surface," *Journal of Applied Physics* **105,** 103114 (2009).

[24] D. J. Rogers, F. H. Teherani, P. Bove, R. McClintock, and M. Razeghi, "Improved LEDs and photovoltaics by hybridization & and nanostructuring," *SPIE Newsroom* 2–5 (2012).

[25] A. Clebsch, "Ueber die Reflexion an einer Kugelfläche," *Journal für Mathematik* **61,** 195–262 (1863).

[26] L. Rayleigh, "On the scattering of light by small particles," *Philosophical Magazine* **41,** 447–454 (1871).

[27] N. Logan, "Survey of some early studies of the scattering of plane waves by a sphere," *Proceedings of the IEEE* **53,** 773–785 (1965).

[28] G. Mie, "Beiträge zur Optik trüber Medien, speziell kolloidaler Metallösungen," *Annalen der Physik, Vierte Folge* **25,** 377–445 (1908).

[29] P. Debye, "Der Lichtdruck auf Kugeln von beliebigem Material," *Annalen der Physik, Vierte Folge* **30,** 57–136 (1909).

[30] M. Born and E. Wolf, *Principles of Optics. Pergamon Press, London 1959.* (Pergamon Press, London, 1959).

[31] C. F. Bohren and D. R. Huffman, *Absorption and Scattering of Light by Small Particles* (Wiley, New York, 1983).

[32] H.C. van de Hulst, *Light Scattering by Small Particles* (Wiley, New York, 1957).

[33] J. D. Jackson, *Classical Electrodynamics Third Edition* (Wiley, 1998).

[34] N. W. Ashcroft and N. D. Mermin, *Solid State Physics* (Brooks Cole, 1976).

[35] K. L. Kelly, E. Coronado, L. L. Zhao, and G. C. Schatz, "The Optical Properties of Metal Nanoparticles: The Influence of Size, Shape, and Dielectric Environment," *Journal of Physical Chemistry B* **107,** 668–677 (2003).

[36] V. Agranovich and D. Mills, *Surface Polaritons - Electromagnetic Waves at Surfaces and Interfaces* (Elsevier Science Ltd, 1982).

[37] J. O. Isard, "The Haven ratio in glasses," *Journal of Non-Crystalline Solids* **246,** 16–26 (1999).

[38] A. L. Stepanov, "Synthesis of silver nanoparticles in dielectric matrix by ion implantation : a review," *Review on Advanced Materials Science* **26,** 1–29 (2010).

[39] A. Miotello, G. De Marchi, G. Mattei, P. Mazzoldi, and A. Quaranta, "Clustering of silver atoms in hydrogenated silver-sodium exchanged glasses," *Applied Physics A: Materials Science & Processing* **70,** 415–419 (2000).

[40] Y. Kaganovskii, A. Lipovskii, M. Rosenbluh, and V. Zhurikhina, "Formation of nanoclusters through silver reduction in glasses: The model," *Journal of Non-Crystalline Solids* **353,** 2263–2271 (2007).

[41] C. G. Bethea, "Electric field induced second harmonic generation in glass," *Applied Optics* **14,** 2435 (1975).

[42] D. Carlson, "Ion Depletion of Glass at a Blocking Anode: I, Theory and Experimental Results for Alkali Silicate Glasses," *Journal of the American Ceramic Society* **57,** 291 (1974).

[43] H. An and S. Fleming, "Near-anode phase separation in thermally poled soda lime glass," *Applied Physics Letters* **88,** 181106 (2006).

[44] O. Deparis, P. G. Kazansky, A. Podlipensky, A. Abdolvand, G. Seifert, and H. Graener, "Evolution of poling-assisted bleaching of metal-doped nanocomposite glass with poling conditions," *Applied Physics Letters* **86,** 261109 (2005).

[45] Y. Quiquempois, a. Kudlinski, G. Martinelli, W. Margulis, and I. C. S. Carvalho, "Near-surface modification of the third-order nonlinear susceptibility in thermally poled Infrasil^{TM} glasses," *Applied Physics Letters* **86,** 181106 (2005).

[46] A. Doi, "Ionic conduction and conduction polarization in oxide glass," *Journal of Materials Science* **22,** 761–769 (1987).

[47] X.-C. Long and S. Brueck, "Large-signal phase retardation with a poled electrooptic fiber," *IEEE Photonics Technology Letters* **9,** 767–769 (1997).

[48] P. Nitzsche, K. Lange, B. Schmidt, S. Grigull, K. Ulrich, B. Thomas, and K. Herzog, "Ion Drift Processes in Pyrex-Type Alkali-Borosilicate Glass during Anodic Bonding," *Journal of Electrochemical Society* **145,** 1755–1762 (1998).

[49] E. C. Ziemath, V. D. Araújo, and C. a. Escanhoela, "Compositional and structural changes at the anodic surface of thermally poled soda-lime float glass," *Journal of Applied Physics* **104,** 054912 (2008).

[50] U. K. Krieger and W. A. Lanford, "Field assisted transport of Na$^+$ ions, Ca^{2+} ions and electrons in commercial soda-lime glass I: experimental," *Journal of Non-Crystalline Solids* **102,** 50–61 (1988).

[51] G. B. Whitham, *Linear and Nonlinear Waves* (Wiley-Interscience, 1999).

[52] K. S. Spiegler and C. D. Coryell, "Electromigration in a Cation Exchange Resin. II. Detailed Analysis of Two-Component Systems," *J. Phys. Chem.* **56,** 106–113 (1952).

[53] A. Podlipensky, A. Abdolvand, G. Seifert, H. Graener, O. Deparis, and P. G. Kazansky, "Dissolution of Silver Nanoparticles in Glass through an Intense dc Electric Field," *The Journal of Physical Chemistry B* **108,** 17699–17702 (2004).

[54] L. Rayleigh, "On the equilibrium of liquid conducting masses charged with electricity," *Philosophical Magazine* **5,** 186–187 (1882).

[55] G. Taylor, "Disintegration of water droplets in an electric field," *Proceedings of the Royal Society A* **280,** 383–397 (1964).

[56] T. Castro, R. Reifenberger, E. Choi, and R. P. Andres, "Size Dependent Melting Temperature of individual nanometer-sized metalic clusters," *Physical Review B* **42,** 8548 (1990).

[57] P. V. Kamat, M. Flumiani, and G. V. Hartland, "Picosecond Dynamics of Silver Nanoclusters . Photoejection of Electrons and Fragmentation," *Journal of Physical Chemistry B* **5647,** 3123–3128 (1998).

[58] A. Podlipensky, A. Abdolvand, G. Seifert, and H. Graener, "Femtosecond laser assisted production of dichroitic 3D structures in composite glass containing Ag nanoparticles," *Applied Physics A* **80,** 1647–1652 (2004).

[59] A. Unal, A. Stalmashonak, H. Graener, and G. Seifert, "Time-resolved investigation of laser-induced shape transformation of silver nanoparticles," *Physical Review B* **80,** 1–7 (2009).

[60] A. Unal, A. Stalmashonak, G. Seifert, and H. Graener, "Ultrafast dynamics of silver nanoparticle shape transformation studied by femtosecond pulse-pair irradiation," *Physical Review B* **79,** 1–7 (2009).

[61] R. R. Letfullin, C. Joenathan, T. F. George, and V. P. Zharov, "Laser-induced explosion of gold nanoparticles: potential role for nanophotothermolysis of cancer.," *Nanomedicine (London, England)* **1,** 473–80 (2006).

[62] A. Stalmashonak, A. Podlipensky, G. Seifert, and H. Graener, "Intensity-driven, laser induced transformation of Ag nanospheres to anisotropic shapes," *Applied Physics B* **94,** 459–465 (2008).

[63] R. G. Forbes, "Field electron and ion emission from charged surfaces: a strategic historical review of theoretical concepts.," *Ultramicroscopy* **95,** 1–18 (2003).

[64] C. G. Sánchez, A. Y. Lozovoi, and A. Alavi, "Field-evaporation from first-principles," *Molecular Physics* **102,** 1045–1055 (2004).

[65] A. Belkhir, "Detailed study of silver metallic film diffusion in a soda-lime glass substrate for optical waveguide fabrication.," *Applied Optics* **41,** 2888–2893 (2002).

[66] R. Oven, M. Yin, and P. A. Davies, "Characterization of planar optical waveguides formed by copper-sodium, electric field assisted, ion exchange in glass," *Journal of Physics D: Applied Physics* **37,** 2207–2215 (2010).

[67] N. Valles-Villarreal, A. Villalobos, and H. Marquez, "Stress in copper ion-exchanged glass waveguides," *Journal of Lightwave Technology* **4,** 1580–1593 (1986).

[68] O. Deparis, P. G. Kazansky, A. Podlipensky, A. Abdolvand, G. Seifert, and H. Graener, "Poling-assisted bleaching of soda-lime float glasses containing silver nanoparticles with a decreasing filling factor across the depth," *Journal of Applied Physics* **100,** 044318 (2006).

[69] M. Leitner, H. Peterlik, B. Sepiol, H. Graener, M. Beleites, and G. Seifert, "Uniformly oriented, ellipsoidal nanovoids in glass created by electric-field-assisted dissolution of metallic nanoparticles," *Physical Review B* **79,** 1–4 (2009).

[70] P. N. Brunkov, V. G. Melekhin, V. Goncharov, A. A. Lipovskii, and M. I. Petrov, "Submicron-resolved relief formation in poled glasses and glass-metal nanocomposites," *Technical Physics Letters* **34,** 1030–1033 (2008).

[71] G. Marchi, F. Caccavale, F. Gonella, G. Mattei, P. Mazzoldi, G. Battaglin, and A. Quaranta, "Silver nanoclusters formation in ion-exchanged waveguides by annealing in hydrogen atmosphere," *Applied Physics A: Materials Science and Processing* **63,** 403–407 (1996).

[72] A. A. Lipovskii, V. G. Melehin, M. I. Petrov, and Y. P. Svirko, "Thermal Electric Field Imprinting Lithography: Fundamentals and Applications," in *Lithography: Principles, Processes and Materials*, T. C. Hennessy, ed. (Nova Science Publishers, New York, 2011), pp. 284.

[73] R. Zia, J. Schuller, A. Chandran, and M. Brongersma, "Plasmonics: the next chip-scale technology," *Materials Today* **9,** 20–27 (2006).

[74] S. I. Bozhevolnyi, V. S. Volkov, E. Devaux, J.-Y. Laluet, and T. W. Ebbesen, "Channel plasmon subwavelength waveguide components including interferometers and ring resonators.," *Nature* **440,** 508–11 (2006).

[75] A. V. Krasavin and A. V. Zayats, "Silicon-based plasmonic waveguides.," *Optics Express* **18,** 11791–9 (2010).

[76] A. Boltasseva, "Plasmonic components fabrication via nanoimprint," *Journal of Optics A: Pure and Applied Optics* **11,** 114001 (2009).

[77] Z. Shi, G. Piredda, A. C. Liapis, M. A. Nelson, L. Novotny, and R. W. Boyd, "Surface-plasmon polaritons on metal – dielectric nanocomposite films," *Optics Letters* **34,** 3535–3537 (2009).

[78] N. Sardana, F. Heyroth, and J. Schilling, "Propagating surface plasmons on nanoporous gold," *Journal of the Optical Society of America B* **29,** 1778 (2012).

[79] D. Lu, J. Kan, E. E. Fullerton, and Z. Liu, "Tunable surface plasmon polaritons in Ag composite films by adding dielectrics or semiconductors," *Applied Physics Letters* **98,** 243114 (2011).

[80] A. A. Lipovskii, V. G. Melehin, M. I. Petrov, Y. P. Svirko, and V. V. Zhurikhina, "Bleaching versus poling: Comparison of electric field induced phenomena in glasses and glass-metal nanocomposites," *Journal of Applied Physics* **109,** 011101 (2011).

[81] A. V. Zayats and D. Richards, *Nano-Optics and Near-Field Optical Microscopy (Artech House)* (Artech House, 2008).

[82] M. Dussauze, E. Kamitsos, E. Fargin, and V. Rodriguez, "Refractive index distribution in the non-linear optical layer of thermally poled oxide glasses," *Chemical Physics Letters* **470,** 63–66 (2009).

[83] A. L. R. Brennand and J. S. Wilkinson, "Planar waveguides in multicomponent glasses fabricated by field-driven differential drift of cations," *Optics Letters* **27,** 906–908 (2002).

[84] M. Beresna, P. G. Kazansky, O. Deparis, I. C. S. Carvalho, S. Takahashi, and A. V. Zayats, "Poling-assisted fabrication of plasmonic nanocomposite devices in glass.," *Advanced materials (Deerfield Beach, Fla.)* **22,** 4368–72 (2010).

[85] U. Kreibig and M. Vollmer, *Optical Properties of Metal Clusters (Springer Series in Materials Science)* (Springer, 1995).

[86] D. A. G. Bruggeman, "Berechnung verschiedener physikalischer Konstanten von heterogenen Substanzen. I. Dielektrizitätskonstanten und Leitfähigkeiten der Mischkörper aus isotropen Substanzen," *Annalen der Physik* **416,** 636–664 (1935).

[87] V. M. Shalaev, ed., *Optical Properties of Nanostructured Random Media* (Springer, Berlin, 2002).

[88] J. C. M. Garnett, "Colours in Metal Glasses and in Metallic Films," *Philosophical Transactions of the Royal Society A: Mathematical, Physical and Engineering Sciences* **203,** 385–420 (1904).

[89] C. Sonnichsen, *Plasmons in metal nanostructures*, PhD thesis (Ludwig-Maximilians-University of Munich, 2001).

[90] J. Turunen and F. Wyrowski, *Diffractive Optics for Industrial and Commercial Applications* (Wiley-VCH, 1998).

[91] P. B. Johnson and R. W. Christy, "Optical Constants of the Noble Metals," *Physical Review B* **6,** 4370–4379 (1972).

[92] M. Czerny, "Uber eine neue Form der Rubenssehen Reststrahlenmethode," *Zeitschrift fur Physik* **16,** 321–331 (1923).

[93] L. Li, "Use of Fourier series in the analysis of discontinuous periodic structures," *Journal of the Optical Society of America A* **13,** 1870–1876 (1996).

[94] L. Li, "New formulation of the Fourier modal method for crossed surface-relief gratings," *Journal of the Optical Society of America A* **14,** 2758 (1997).

[95] M. G. Moharam, E. B. Grann, D. a. Pommet, and T. K. Gaylord, "Formulation for stable and efficient implementation of the rigorous coupled-wave analysis of binary gratings," *Journal of the Optical Society of America A* **12,** 1068 (1995).

[96] K. L. Kliewer and R. Fuchs, "Optical Modes of Vibration in an Ionic Crystal Salb Including Retardation. I. Nonradiative Region.," *Physical Review* **144,** 495 (1966).

[97] R. Fuchs, K. L. Kliewer, and W. Pardee, "Optical Properties of an Ionic Crystal Slab," *Physical Review* **150,** 589–596 (1966).

[98] K. L. Kliewer and R. Fuchs, "Optical Modes of Vibration in an Ionic Crystal Slab Including Retardation. II. Radiative Region," *Atomic Energy* **150,** 573 (1966).

[99] Y. Liu and X. Zhang, "Metamaterials: a new frontier of science and technology.," *Chemical Society reviews* **40,** 2494–507 (2011).

[100] T. W. Ebbesen, H. J. Lezec, H. F. Ghaemi, T. Thio, and P. A. Wolff, "Extraordinary optical transmission through subwavelength hole arrays," *Nature* **391,** 667–669 (1998).

[101] F. J. García de Abajo, "Colloquium: Light scattering by particle and hole arrays," *Reviews of Modern Physics* **79,** 1267–1290 (2007).

[102] I. Iorsh, A. Orlov, P. Belov, and Y. Kivshar, "Interface modes in nanostructured metal-dielectric metamaterials," *Applied Physics Letters* **99,** 151914 (2011).

Mihail Petrov

Glass-metal nanocomposites for photonics applications

This work is dedicated to theoretical and experimental investigations of electric field induced effects in glasses and glass-metal nanocomposites. Basing on the effect of electric field assisted dissolution of metal nanoparticles 1D and 2D optical subwavelength periodic structures were fabricated. According to theoretical calculations optical properties of nanocomposite-based diffraction gratings can be controlled with nanocomposite properties that gives additional degree of freedom to engineer their diffraction patterns.

UNIVERSITY OF
EASTERN FINLAND

Publications of the University of Eastern Finland
Dissertations in Forestry and Natural Sciences

ISBN: 978-952-61-1072-1 (printed)
ISSNL: 1798-5668
ISSN: 1798-5668
ISBN: 978-952-61-1073-8 (pdf)
ISSNL: 1798-5668
ISSN: 1798-5676